

Calibrating Local Volatility Models with Stochastic Drift and Diffusion*

Orcan Ögetbil[†], Narayan Ganesan[‡], and Bernhard Hientzsch[§]

Corporate Model Risk, Wells Fargo Bank

Abstract

We propose Monte Carlo calibration algorithms for three models: local volatility with stochastic interest rates, stochastic local volatility with deterministic interest rates, and finally stochastic local volatility with stochastic interest rates. For each model, we include detailed derivations of the corresponding SDE systems, and list the required input data and steps for calibration. We give conditions under which a local volatility can exist given European option prices, stochastic interest rate model parameters, and correlations. The models are posed in a foreign exchange setting. The drift term for the exchange rate is given as a difference of two stochastic short rates, domestic and foreign, each modeled by a Gaussian one-factor model with deterministic shift (G1++) process. For stochastic volatility, we model the variance for the exchange rate by a Cox-Ingersoll-Ross (CIR) process. We include tests to show the convergence and the accuracy of the proposed algorithms.

1 Introduction

In quantitative finance, considerable amount of research focuses on modeling the market-observed smile of the implied volatility surface. There are competing approaches to tackle this problem. Most notably, stochastic volatility and local volatility models are often applied in practice to imitate the market-observed smile. Stochastic volatility models aim to capture the volatility dynamics observed in the market. While such models often capture the implied volatilities in certain tenor and strike ranges well, there are often ranges that are not repriced well. Moreover, the parametric structure of these models makes proper calibration computationally challenging. The local volatility models are simpler due to their non-parametric nature; and they are constructed to fit completely arbitrage-free implied volatility surfaces. However, they fail to capture the proper dynamics of implied volatilities,

*Electronic version of the article published as International Journal of Theoretical and Applied Finance, Volume No. 25, Issue No. 02, Article No. 2250011, Year 2022 <https://dx.doi.org/10.1142/S021902492250011X> ©World Scientific Publishing Company <https://www.worldscientific.com/worldscinet/ijtaf>

[†]orcan.ogetbil@wellsfargo.com

[‡]narayan.ganesan@wellsfargo.com

[§]bernhard.hientzsch@wellsfargo.com

as they construct a static local volatility surface, which inherently assumes deterministic spot volatility for the underlying process. These shortcomings lead practitioners to combine them in unified frameworks, called *stochastic local volatility* models, with the intention of combining the advantages of both approaches. The combined model is of special interest to the financial industry, as it would provide a methodology to work with a more complete set of risk factors associated with exotic instruments, such as options on exchange rates, foreign stocks, quantoes and baskets.

Dupire’s local volatility model [1, 2] constructs a unique diffusion process that is consistent with the European vanilla option market quotes. Being calibrated to vanilla option quotes, the local volatility surface has become a standard tool to capture the risk-neutral marginal distributions of the underliers implied by market European option price quotes, and is being utilized by practitioners for pricing and risk-assessment of more exotic instruments. In its original formulation, the local volatility model assumes deterministic drift and diffusion terms. In our work, we relax both of these constraints in turn, and study the generalizations of the local volatility model first under a drift that is the difference between two stochastic short rates, then under stochastic diffusion, and eventually under both stochastic drift and stochastic diffusion. While we base our set up in foreign exchange context with the foreign exchange rate, the domestic and base short rates as the risk drivers, our results can be applied in equity or commodity contexts. The theoretical setup and algorithms presented in the paper can be simplified with minimal effort to the cases where the drift is modeled more simplistically with a single short rate driver.

The theoretical framework for extending the local volatility model with a single stochastic rate was presented in [3]. Calibration of this model using finite difference and Monte Carlo (MC) methods was discussed in [4, 5]. As a further extension, [6] studies the model with two stochastic interest rates.

Stochastic volatility models embody a spot volatility or variance process that is correlated to the underlying asset. Popular choices are the Heston model [7] with variance following a Cox-Ingersoll-Ross (CIR) process [8], and the Stein-Stein model [9, 10] with volatility following an arithmetic Ornstein-Uhlenbeck process [11]. Both models admit closed form solutions, at least in their constant parameter formulations, for pricing European vanilla options. [3] proposes an extension to stochastic volatility models with a stochastic interest rate. A more common extension is to join the local volatility with the stochastic volatility or variance in the diffusion term of the stochastic differential equation (SDE) to form a stochastic local volatility model. In the literature, the theoretical framework for stochastic local volatility has been studied in several forms with varying degrees of model complexity. The “unified theory of volatility” from [12] imposes dynamics on local variances, whereas [13] focus on modeling the stochastic evolution of the local volatility surface rather than of the spot volatility. [14] proposes a further extension to incorporate jumps in the model. Calibration algorithms for several forms of stochastic local volatility models have been introduced. [15] implement a trinomial tree whereas, [16] utilize particle methods on McKean nonlinear SDEs on general volatility models, [17, 18] solve a forward Kolmogorov PDE. The bootstrapping Monte Carlo method proposed by [19] simplifies the model by Markovian projection. Our approach of simulating the full stochastic local volatility model in our work paves the way to further extend the model to incorporate stochastic rates.

We use a number of acronyms for the models under consideration for easy reference.

The standard Dupire local volatility model where the drift is the difference between two deterministic rates is denoted by LV2DR. The stochastic rates extension of this model is LV2SR, whereas the stochastic local volatility extension is SLV2DR. The full model with stochastic rates and stochastic local volatility is referred to as SLV2SR.

While this paper reviews and makes use of existing findings and algorithms in part, to our knowledge, the following are our novel contributions: SLV2SR model; complete derivations of the SDE systems that are used during Monte Carlo calibration for all three models: LV2SR, SLV2DR, SLV2SR; presentation of Monte Carlo calibration algorithms for the SLV2DR and SLV2SR models; and convergence and accuracy studies of all calibration algorithms presented.

The structure of this paper is as follows. We end this section by reviewing the theoretical foundations that our models will be based on. In Section 2, we give a detailed description of the algorithm to calibrate the local volatility model subject to stochastic interest rates (LV2SR), including derivations of the relevant formulas and SDEs in forward measure. Section 3 describes the two-fold calibration algorithm of the stochastic local volatility model (SLV2DR): First the underlying Heston model is calibrated to match near at-the-money forward (ATMF) market quotes; then the leverage function is calibrated to the entire implied volatility surface. Section 4 blends the algorithms from the previous sections to develop a calibration algorithm for our ultimate model: stochastic local volatility with stochastic interest rates (SLV2SR). As the models being discussed are built on top of each other, the calibration algorithm for the SLV2SR model references and uses the results of the algorithms for calibrating the simpler models in earlier sections. In this paper stochastic interest rates are modeled by Gaussian one-factor model with deterministic shift (G1++) short rate processes. Other short rate models can be adapted to our framework as well, as our methodology is not tightly coupled with the choice for the type of the short rate process. Each of these sections are accompanied by tests that measure the convergence and the accuracy of the calibrated models. We use EURUSD market data as of 2020-04-30 in our calibration and simulation tests. In Section 5 we summarize our findings and exhibit a study to compare the calibrated models. A proves a few technical lemmas and provides some computations used in the paper.

We work in the standard probability space setting that can be found in most mathematical finance textbooks. Here we briefly discuss the relevant constructs for the sake of clarity, and for detail we refer to [20]. We consider the measurable space (Ω, \mathcal{F}) , where the sample space Ω with outcome elements ω governs the uncertainty; \mathcal{F} , as a σ -algebra on Ω , controls information availability. Together with a probability measure \mathbb{P} , they form the probability space $(\Omega, \mathcal{F}, \mathbb{P})$. The expectation operator for the measure \mathbb{P} is denoted by $\mathbf{E}^{\mathbb{P}}$. The filtration $\{\mathcal{F}_t, t \geq 0\}$, defined as a set over subalgebras \mathcal{F}_t of \mathcal{F} satisfying $\mathcal{F}_s \subseteq \mathcal{F}_t$ for $s \leq t$, models the information arrivals at different times.

We consider the setup where the filtration $\{\mathcal{F}_t, t \geq 0\}$ is generated by M independent Brownian motions $(W_t^m), m = 1, \dots, M$, under \mathbb{P} . We can formulate a model with \mathcal{F}_t -measurable stochastic processes (X_t^n) that are driven by (W_t^m)

$$dX_t^n = \mu^n(t, \omega)dt + \sum_{m=1}^M \sigma^{nm}(t, \omega)dW_t^m, \quad n = 1, \dots, N,$$

by means of \mathcal{F}_t -measurable drift $\mu^n(t, \omega)$ and diffusion $\sigma^{nm}(t, \omega)$ functions that for all t

satisfy the integrability conditions

$$\int_0^t |\mu^n(s, \omega)| ds < \infty,$$

$$\int_0^t \sum_{m=1}^M |\sigma^{nm}(s, \omega)|^2 ds < \infty,$$

almost surely. The stochastic processes that we are primarily considering in this paper are exchange rate, stochastic volatility/variance, domestic and foreign interest rates. Other tradable assets we consider are domestic and foreign money market accounts, which as numéraires define the domestic and foreign risk neutral measures \mathbb{Q}^{DRN} and \mathbb{Q}^{FRN} respectively; and domestic zero coupon bond maturing at future time T , which as numéraire defines the domestic T -forward measure \mathbb{Q}^T .

The discounted asset values are martingales under the risk neutral measure they are denominated in. It is convenient to formulate the stochastic processes we will study in risk neutral measures, in which they can be written in their canonical forms, driven by a single Brownian motion. For example, a process (X_t^n) is driven by the Brownian motion $(W_t^{n(\text{DRN})})$ under the domestic risk neutral measure as

$$dX_t^n = \tilde{\mu}^n(t, \omega)dt + \tilde{\sigma}^n(t, \omega)dW_t^{n(\text{DRN})}.$$

In this formulation the Brownian motions $(W_t^{n(\text{DRN})})$ of each process (X_t^n) are not nec-

Table 1.1: The processes and the corresponding correlated Brownian motions under the domestic risk-neutral measure

	$N (= M)$	$\{X_t^n\}$	$\{W_t^{n(\text{DRN})}\}$
LV2DR	1	S_t	$W_t^{S(\text{DRN})}$
LV2SR	3	S_t, r_t^d, r_t^f	$W_t^{S(\text{DRN})}, W_t^{d(\text{DRN})}, W_t^{f(\text{DRN})}$
SLV2DR	2	S_t, U_t	$W_t^{S(\text{DRN})}, W_t^{U(\text{DRN})}$
SLV2SR	4	S_t, U_t, r_t^d, r_t^f	$W_t^{S(\text{DRN})}, W_t^{U(\text{DRN})}, W_t^{d(\text{DRN})}, W_t^{f(\text{DRN})}$

essarily uncorrelated. Note that any model $(X_t^n), n = 1, \dots, N$, with correlated Brownian motions can be rewritten as a model with uncorrelated Brownian motions, absorbing any correlation into the diffusion terms. In this paper we specify the stochastic processes for the exchange rate (S_t) under various models. LV2SR and SLV2SR models specify the domestic short rate (r_t^d) and the foreign short rate (r_t^f) processes; and SLV2DR and SLV2SR models further specify the exchange rate variance process (U_t) . Under domestic risk neutral measure \mathbb{Q}^{DRN} , these processes are driven by the correlated Brownian motions $(W_t^{S(\text{DRN})}), (W_t^{d(\text{DRN})}), (W_t^{f(\text{DRN})}),$ and $(W_t^{U(\text{DRN})}),$ respectively. Table 1.1 summarizes the models under consideration. A sample implementation of the calibration algorithms presented in the following sections can be found at the Github repository https://github.com/oge-t/subtle_smile.

2 Local Volatility Model with Stochastic Rates (LV2SR)

2.1 Setup

Let (S_t) be the exchange rate, that is the amount of domestic currency needed to buy one unit of foreign currency. In the domestic risk neutral measure \mathbb{Q}^{DRN} the exchange rate is assumed to follow the LV2SR local volatility model,

$$dS_t = \left[r_t^d - r_t^f \right] S_t dt + \sigma(S_t, t) S_t dW_t^{S(\text{DRN})}, \quad (2.1)$$

where $\sigma(S_t, t) > 0$ is the state dependent diffusion coefficient that is commonly referred to as *local volatility*, and (S_t) is denominated in domestic currency. The domestic short rate (r_t^d) and the foreign short rate (r_t^f) follow G1++ processes. In particular, the domestic short rate evolves in domestic risk neutral measure as

$$\begin{aligned} r_t^d &= x_t^d + \phi_t^d, \\ dx_t^d &= -a_t^d x_t^d dt + \sigma_t^d dW_t^{d(\text{DRN})}, \end{aligned} \quad (2.2)$$

whereas the foreign short rate evolves in foreign risk neutral measure \mathbb{Q}^{FRN} as

$$\begin{aligned} r_t^f &= x_t^f + \phi_t^f, \\ dx_t^f &= -a_t^f x_t^f dt + \sigma_t^f dW_t^{f(\text{FRN})}. \end{aligned} \quad (2.3)$$

Here ϕ_t^i are the shift functions that are calibrated to market yield curves; $a_t^i \geq 0$ are the mean reversion coefficients, and $\sigma_t^i > 0$ are the volatility coefficients, with $i = d, f$.

Our derivations and computations assume constant coefficients of correlation between the returns of the underlying assets; however we note that it is straightforward to generalize our findings to more advanced models with time-dependent or even stochastic coefficients of correlation.

2.1.1 Domestic risk neutral measure

The first step is to derive the evolution of the foreign short rate in the domestic risk neutral measure. For now assume that the evolution of the foreign short rate in domestic risk neutral measure has the form

$$dx_t^f = g(\cdot, t) dt + \sigma_t^f dW_t^{f(\text{DRN})} \quad (2.4)$$

for some drift function $g(\cdot, t)$ of the underlying assets of the SDE system and time that we are going to determine.

For any asset V_t denominated in domestic currency, the discounted asset price is a martingale under the domestic risk neutral measure. Defining the domestic money market account as $B_t^d = \exp[\int_0^t r_u^d du]$, we have

$$\frac{V_0}{B_0^d} = V_0 = \mathbf{E}^{\mathbb{Q}^{\text{DRN}}} \left[\frac{V_t}{B_t^d} \right].$$

Likewise, the discounted value of $\frac{V_t}{S_t}$, that is the price of the asset V_t denominated in the foreign currency, is a martingale under the foreign risk neutral measure. Defining the foreign money market account as $B_t^f = \exp[\int_0^t r_u^f du]$, we have

$$\frac{V_0}{S_0 B_0^f} = \frac{V_0}{S_0} = \mathbf{E}^{\mathbb{Q}^{\text{FRN}}} \left[\frac{V_t}{S_t B_t^f} \right].$$

Therefore the Radon-Nikodym derivative [20] writes

$$\frac{d\mathbb{Q}^{\text{FRN}}}{d\mathbb{Q}^{\text{DRN}}} = \frac{\frac{V_t}{B_t^d} \frac{V_0}{S_0}}{V_0 \frac{V_t}{S_t B_t^f}} = \frac{S_t B_t^f}{S_0 B_t^d}. \quad (2.5)$$

The exchange rate process (2.1) is an extension of the geometric Brownian motion SDE with time-dependent coefficients r_t^d , r_t^f , and time- and space-dependent coefficient $\sigma(S_t, t)$, with the solution that describes its evolution from its spot value S_0 ,

$$\begin{aligned} S_t &= S_0 \exp \left[\int_0^t \left(r_u^d - r_u^f - \frac{\sigma^2(S_u, u)}{2} \right) du + \int_0^t \sigma(S_u, u) dW_u^{S(\text{DRN})} \right] \\ &= S_0 \frac{B_t^d}{B_t^f} \exp \left[-\frac{1}{2} \int_0^t \sigma^2(S_u, u) du + \int_0^t \sigma(S_u, u) dW_u^{S(\text{DRN})} \right]. \end{aligned}$$

Thus, the Radon-Nikodym derivative (2.5) becomes

$$\frac{d\mathbb{Q}^{\text{FRN}}}{d\mathbb{Q}^{\text{DRN}}} = \exp \left[-\frac{1}{2} \int_0^t \sigma^2(S_u, u) du + \int_0^t \sigma(S_u, u) dW_u^{S(\text{DRN})} \right]. \quad (2.6)$$

Then, according to the Girsanov theorem

$$dW_t^{S(\text{FRN})} = dW_t^{S(\text{DRN})} - \sigma(S_t, t) dt \quad (2.7)$$

is a Brownian motion under the foreign risk neutral measure \mathbb{Q}^{FRN} .

Let ρ_{Sf} be the coefficient of correlation between the Brownian motions $(W_t^{S(\text{FRN})})$ and $(W_t^{f(\text{FRN})})$, that is $d\langle W^{S(\text{FRN})}, W^{f(\text{FRN})} \rangle_t = \rho_{Sf} dt$. Following Lemma A.1, the foreign short rate process (2.4) evolves in foreign risk neutral measure \mathbb{Q}^{FRN} as

$$dx_t^f = \left[g(\cdot, t) + \rho_{Sf} \sigma_t^f \sigma(S_t, t) \right] dt + \sigma_t^f dW_t^{f(\text{FRN})}. \quad (2.8)$$

Comparing (2.3) and (2.8), we find that

$$g(\cdot, t) = -a_t^f x_t^f - \rho_{Sf} \sigma_t^f \sigma(S_t, t).$$

Collectively, we can write the three processes in the domestic risk neutral measure as

$$\begin{aligned} dS_t &= \left[r_t^d - r_t^f \right] S_t dt + \sigma(S_t, t) S_t dW_t^{S(\text{DRN})}, \\ dx_t^d &= -a_t^d x_t^d dt + \sigma_t^d dW_t^{d(\text{DRN})}, \quad r_t^d = x_t^d + \phi_t^d, \\ dx_t^f &= \left[-a_t^f x_t^f - \rho_{Sf} \sigma_t^f \sigma(S_t, t) \right] dt + \sigma_t^f dW_t^{f(\text{DRN})}, \quad r_t^f = x_t^f + \phi_t^f. \end{aligned} \quad (2.9)$$

2.1.2 Domestic T -forward measure

For computational ease, that is to decouple the discounting terms from expectations, we would like to transform (2.9) to the domestic T -forward measure. We take the zero coupon bond $P^d(t, T)$ maturing at time T as the numéraire. We have $P^d(T, T) = 1$. Under the measure \mathbb{Q}^T defined by this numéraire, the discounted price of an asset is a martingale,

$$\frac{V_0}{P^d(0, T)} = \mathbf{E}^{\mathbb{Q}^T} \left[\frac{V_T}{P^d(T, T)} \right] = \mathbf{E}^{\mathbb{Q}^T} [V_T].$$

We arrive at the following Radon-Nikodym derivative,

$$\frac{d\mathbb{Q}^T}{d\mathbb{Q}^{\text{DRN}}} = \frac{\frac{V_T}{B_T^d} \frac{V_0}{P^d(0, T)}}{V_0 V_T} = \frac{1}{B_T^d P^d(0, T)} = \frac{\exp \left[- \int_0^T r_u^d du \right]}{P^d(0, T)}. \quad (2.10)$$

Since the domestic short rate follows a G1++ process, this expression can be written as (see Lemma A.2 for proof)

$$\frac{d\mathbb{Q}^T}{d\mathbb{Q}^{\text{DRN}}} = \exp \left[- \int_0^T \sigma_u^d b^d(u, T) dW_u^{d(\text{DRN})} - \frac{1}{2} \int_0^T \left(\sigma_u^d b^d(u, T) \right)^2 du \right], \quad (2.11)$$

with

$$b^d(t, T) \equiv \int_t^T e^{-\int_t^v a_z^d dz} dv.$$

Then, by Girsanov theorem

$$dW_t^{d(T)} = dW_t^{d(\text{DRN})} + b^d(t, T) \sigma_t^d dt \quad (2.12)$$

is a Brownian motion under the domestic T -forward measure \mathbb{Q}^T . This allows us to write down the domestic short rate process (2.2) as

$$dx_t^d = \left[-a_t^d x_t^d - b^d(t, T) (\sigma_t^d)^2 \right] dt + \sigma_t^d dW_t^{d(T)}. \quad (2.13)$$

Let ρ_{Sd} be the coefficient of correlation between the Brownian motions $(W_t^{S(\text{DRN})})$ and $(W_t^{d(\text{DRN})})$, that is $d\langle W^{S(\text{DRN})}, W^{d(\text{DRN})} \rangle_t = \rho_{Sd} dt$. Following Lemma A.1, the exchange rate process (2.1) evolves in domestic T -forward measure \mathbb{Q}^T as

$$dS_t = \left[r_t^d - r_t^f - \rho_{Sd} b^d(t, T) \sigma_t^d \sigma(S_t, t) \right] S_t dt + \sigma(S_t, t) S_t dW_t^{S(T)}. \quad (2.14)$$

Finally, let ρ_{df} be the coefficient of correlation between the Brownian motions $(W_t^{d(\text{DRN})})$ and $(W_t^{f(\text{DRN})})$, that is $d\langle W^{d(\text{DRN})}, W^{f(\text{DRN})} \rangle_t = \rho_{df} dt$. Following Lemma A.1, the foreign short rate process from (2.9) evolves in domestic T -forward measure \mathbb{Q}^T as

$$dx_t^f = \left[-a_t^f x_t^f - \rho_{Sf} \sigma_t^f \sigma(S_t, t) - \rho_{df} b^d(t, T) \sigma_t^d \sigma_t^f \right] dt + \sigma_t^f dW_t^{f(T)}. \quad (2.15)$$

Collecting everything,

$$\begin{aligned}
dS_t &= \left[r_t^d - r_t^f - \rho_{Sd} b^d(t, T) \sigma_t^d \sigma(S_t, t) \right] S_t dt + \sigma(S_t, t) S_t dW_t^{S(\mathbb{T})}, \\
dx_t^d &= \left[-a_t^d x_t^d - b^d(t, T) (\sigma_t^d)^2 \right] dt + \sigma_t^d dW_t^{d(\mathbb{T})}, \quad r_t^d = x_t^d + \phi_t^d, \\
dx_t^f &= \left[-a_t^f x_t^f - \rho_{Sf} \sigma_t^f \sigma(S_t, t) - \rho_{df} b^d(t, T) \sigma_t^d \sigma_t^f \right] dt + \sigma_t^f dW_t^{f(\mathbb{T})}, \quad r_t^f = x_t^f + \phi_t^f
\end{aligned} \tag{2.16}$$

describe the evolutions of the exchange rate, domestic short rate, and foreign short rate processes under the domestic T -forward measure \mathbb{Q}^T . Note that the above SDE system is different than what is given in [6].

2.2 Calibration of Local Volatility

The standard formulation of the local volatility model [1, 2] with deterministic interest rates has been studied extensively in the literature. The local volatility surface can be computed from a call option price surface that can be constructed by market quotes of call option prices $C = C(K, T)$ as [21]

$$\sigma_{\text{LV}}^2 \text{ (deterministic rates)} = \frac{\frac{\partial C}{\partial T} + (r_T^d - r_T^f) K \frac{\partial C}{\partial K} + r_T^f C}{\frac{1}{2} K^2 \frac{\partial^2 C}{\partial K^2}}. \tag{2.17}$$

When the interest rates have stochastic dynamics, the above equation generalizes to [22]

$$\sigma_{\text{LV}}^2 \text{ (stochastic rates)} = \frac{\frac{\partial C}{\partial T} - P^d(0, T) \mathbf{E}^{\mathbb{Q}^T} \left[(K r_T^d - S_T r_T^f) \mathbf{1}_{S_T > K} \right]}{\frac{1}{2} K^2 \frac{\partial^2 C}{\partial K^2}}. \tag{2.18}$$

Here $P^d(0, T)$ is the time zero value of a zero coupon bond expiring at time T , which can be extracted from the input domestic discount factor curve. The expectation is taken under the domestic T -forward measure \mathbb{Q}^T .

One can show that when the rates (r_t^d) , (r_t^f) are deterministic ($\sigma_t^d \rightarrow 0, \sigma_t^f \rightarrow 0$), (2.18) reduces to (2.17). In the stochastic case, however, this expectation does not have a known analytical solution and needs to be evaluated numerically. Below, we demonstrate our methods for evaluating this expectation by Monte Carlo simulation.

The evaluation of the local volatility requires the construction of the *call price surface* interpolator in this formulation. The interpolator must be able to evaluate the partial derivatives appearing in the above local volatility expressions¹. This surface and its t - and K -derivatives will be evaluated at a given grid to generate the local volatility surface using equations (2.17) or (2.18).

As the FX volatility market data is usually given in terms of risk-reversals and butterflies, and represented as some *implied volatility surface* form with appropriate interpolation, we choose to write the Dupire's equations in the total implied variance parametrization.

¹In our implementation, the interpolator is constructed as clamped cubic spline in strike direction, and linear spline in time direction. The derivatives are computed analytically on the splines. Expiries are uniformly spaced. At each expiry the strikes range 3.5 standard deviations (based on the corresponding implied volatility) away from at-the-money-forward strike, and are uniformly spaced in log-moneyness.

Comparing the calibration routines on various sets of initial market data, we found that in the wings of the surface, the total implied variance formulation typically performs better than the call surface formulation. In practice, market data is usually available in the form of parametrized or dense implied volatility surfaces that are calibrated with such penalty functions that force the total implied variance to increase monotonically as a function of time. By construction, interpolating the total implied variance surface and using these values in the Dupire formula avoids calendar spread arbitrage.

Following the conventions of [21], the total implied variance w is parametrized in terms of the log-moneyness $y(K, T) = \log \frac{K}{F_T}$ and time T , with forward asset price $F_T = S_0 \frac{P^f(0, T)}{P^d(0, T)}$, as $w(y(K, T), T) = \Sigma(K, T)^2 T$ where $\Sigma(K, T)$ is the market implied volatility at strike K and maturity T .

In the deterministic interest rates case, the Dupire's equation (2.17) reduces to [21]

$$\sigma_{\text{LV (deterministic rates)}}^2 = \frac{\frac{\partial w}{\partial T}}{1 - \frac{y}{w} \frac{\partial w}{\partial y} + \frac{1}{2} \frac{\partial^2 w}{\partial y^2} + \frac{1}{4} \left(\frac{\partial w}{\partial y} \right)^2 \left(-\frac{1}{4} - \frac{1}{w} + \frac{y^2}{w^2} \right)}. \quad (2.19)$$

Meanwhile, in the stochastic interest rates case, the equation (2.18) becomes [22]

$$\sigma_{\text{LV (stochastic rates)}}^2 = \frac{\frac{\partial C_{\text{BS}}}{\partial T} - P^d(0, T) \mathbf{E}^{\mathbb{Q}^T} \left[(K r_T^d - S_T r_T^f) \mathbf{1}_{S_T > K} \right]}{\frac{\partial C_{\text{BS}}}{\partial w} \left[1 - \frac{y}{w} \frac{\partial w}{\partial y} + \frac{1}{2} \frac{\partial^2 w}{\partial y^2} + \frac{1}{4} \left(\frac{\partial w}{\partial y} \right)^2 \left(-\frac{1}{4} - \frac{1}{w} + \frac{y^2}{w^2} \right) \right]}, \quad (2.20)$$

where the Black-Scholes model price $C_{\text{BS}} = C_{\text{BS}}(P^d(0, T) F_T, y, w)$ and its derivatives are given by

$$\begin{aligned} C_{\text{BS}}(P^d(0, T) F_T, y, w) &= P^d(0, T) F_T [N(d_1) - e^y N(d_2)], \\ \frac{\partial C_{\text{BS}}}{\partial w} &= \frac{1}{2} P^d(0, T) F_T e^y N'(d_2) w^{-\frac{1}{2}}, \\ \frac{\partial C_{\text{BS}}}{\partial y} &= -P^d(0, T) F_T e^y N(d_2), \\ \frac{\partial C_{\text{BS}}}{\partial T} &= -f^f(0, T) C_{\text{BS}} + \frac{\partial C_{\text{BS}}}{\partial w} \frac{\partial w}{\partial T} \\ &\quad + \left(\frac{\partial C_{\text{BS}}}{\partial y} + \frac{\partial C_{\text{BS}}}{\partial w} \frac{\partial w}{\partial y} \right) (f^f(0, T) - f^d(0, T)). \end{aligned} \quad (2.21)$$

Here the instantaneous forward rate is defined as $f^i(0, T) \equiv -\frac{\partial \log P^i(0, T)}{\partial T} = -\frac{1}{P^i(0, T)} \frac{\partial P^i(0, T)}{\partial T}$, with $i = d, f$. Moreover $N(\cdot)$ is the cumulative Gaussian probability distribution function; $d_1 = -yw^{-\frac{1}{2}} + \frac{1}{2}w^{\frac{1}{2}}$, and $d_2 = d_1 - w^{\frac{1}{2}}$. r_T^d and r_T^f are the time T values of the domestic and foreign short rates. Similar to the call price surface formulation, equation (2.20) reduces to (2.19) in the deterministic interest rates limit. Analogous to the call price formulation case, the evaluation of the local volatility requires the construction of the *total implied variance surface*.

Dupire's equations (2.18) and (2.20) use the local volatility on both sides since the computation of the expectation on the right hand side is under the dynamics that involves

the local volatility function. This can be used to define iterative approaches. We found that the bootstrapping approach presented below typically yields satisfactory results without any iterative refinement.

Inputs for calibration Our calibration routine expects the following quantities as input for local volatility calibration:

- Spot FX rate S_0
- Market implied volatility $\Sigma(K, t)$ for FX rate
- Market yield curves $P^d(0, t)$ and $P^f(0, t)$
- For both domestic and foreign rates, G1++ model parameters mean reversion, volatility and shift function calibrated to market data²
- Coefficients of correlation between the underlying assets: the FX rate, the domestic and foreign short rates

Steps for calibration In our framework, we calibrate the local volatility surface time slice by time slice, in a bootstrapping fashion. Let $t_i; i = 1, \dots, n$ be the increasing sequence of (positive) times where we will perform the calibration.

1. Using the market implied volatility $\Sigma(K, t)$, generate a vanilla call option price surface $C(K, t)$ interpolator or a total implied variance surface $w(y, t)$ interpolator. The interpolator must be able to compute the partial derivatives appearing in the local volatility expressions.
2. For the first time slice t_1 , evaluate the deterministic equation (2.17) or (2.19) to compute the FX local volatilities for a predetermined range of strikes. This step requires no Monte Carlo simulation. As a result, obtain local volatility values to be used in the simulation until time t_2 in the subsequent calibration steps.
3. For each of the subsequent time slices $t_j, j > 1$, simulate the SDE system (2.16) up to time t_j . Compute the Monte Carlo estimate for the expectation appearing in (2.18) or (2.20) for a predetermined range of strikes. Use these equations to obtain the local volatility values. These local volatility values will be used during subsequent simulation steps from time t_j to time t_{j+1} . This step is first performed with $j = 2$ and is then repeated for the remaining time slices.

The strike grid can be chosen to be uniform across all calibration time slices. In this approach, however, the strike grid needs to be sufficiently large to cover attainable values of the FX rate at long expiries. This in turn would result in unreliable local volatility values at short expiries and strikes in the far wings. To overcome this problem, we suggest using a more adequate strike grid at each calibration time slice, e.g. one that spans a predetermined number of standard deviations away from the ATMF strike value. Another plausible approach is choosing the strike grid to cover the range of strikes that the implied volatility surface is calibrated to, if this information is available.

²See [23] for example calibration methods for both constant and time dependent cases.

2.3 Calibration and Simulation Tests

In order to test the validity of the calibrated local volatility surface, one needs to use it for pricing. The prices generated by Monte Carlo simulation by this method, however, have two sources of Monte Carlo errors. First, the estimation of the expectations appearing in (2.18) or (2.20) is subject to Monte Carlo error. Second, the evaluation of the Monte Carlo average of the payoffs computed during the pricing introduces an additional source of error. Keeping the number of paths high in one of these two steps will allow us to study the convergence of the other.

For both calibration and pricing, we also generate the antithetic conjugate paths to reduce the variance. Therefore when we talk about a simulation with N as the number of paths, the actual total number of paths simulated is $2N$.

The G1++ model parameters we use as input are summarized in Table 2.1. The coefficients of correlation are given by $\rho_{Sd} = 0.166$, $\rho_{Sf} = 0.551$, $\rho_{df} = 0.161$. The domestic T -forward measure SDE system (2.16) is simulated via forward Euler discretization in both calibration and pricing steps. We vary the number of paths used during calibration while we fix the number of paths for the pricing simulation at 100,000.

Table 2.1: G1++ model parameters for the domestic currency USD and foreign currency EUR used as input data in our calibration routine. In our implementation these are interpolated piecewise constantly with left endpoints.

t	σ_t^d	σ_t^f	a_t^d	a_t^f
0	0.00956	0.00820	0.02	0.02
0.24	0.00881	0.00777		
0.50	0.00851	0.00754		
0.99	0.00804	0.00725		
1.99	0.00818	0.00713		
2.99	0.00816	0.00747		
4.99	0.00810	0.00740		
9.99	0.00818	0.00771		
14.99	0.00818	0.00771		

In this test, we use the total implied variance formulation (2.20). The Monte Carlo estimate for the local volatility is given by

$$\hat{\sigma}_{LV}^2 = \frac{\frac{\partial C_{BS}}{\partial T} - P^d(0, T)\hat{E}}{\frac{\partial C_{BS}}{\partial w} \left[1 - \frac{y}{w} \frac{\partial w}{\partial y} + \frac{1}{2} \frac{\partial^2 w}{\partial y^2} + \frac{1}{4} \left(\frac{\partial w}{\partial y} \right)^2 \left(-\frac{1}{4} - \frac{1}{w} + \frac{y^2}{w^2} \right) \right]},$$

where \hat{E} is the Monte Carlo estimate for the expectation appearing in (2.20). In this formulation, the Monte Carlo error $\delta \hat{E}$ of this estimate translates to the error in local volatility as

$$\delta \hat{\sigma}_{LV} = \left| \frac{P^d(0, T)\delta \hat{E}}{2\hat{\sigma}_{LV} \frac{\partial C_{BS}}{\partial w} \left[1 - \frac{y}{w} \frac{\partial w}{\partial y} + \frac{1}{2} \frac{\partial^2 w}{\partial y^2} + \frac{1}{4} \left(\frac{\partial w}{\partial y} \right)^2 \left(-\frac{1}{4} - \frac{1}{w} + \frac{y^2}{w^2} \right) \right]} \right|.$$

For every point of the calibrated surface, we estimate the Monte Carlo error in the local volatility values. In the end we price with three volatility surfaces: the original calibrated surface, the original calibrated surface bumped down by 2 Monte Carlo errors, and the original calibrated surface bumped up by 2 Monte Carlo errors.

The total implied variance interpolator has a time slice every 0.05 years, and 100 log-moneynesses per slice. The log-moneyness points are spanned uniformly over 3.5 standard deviations from the ATMF strike value for each slice. Similarly, the local volatility surface is calibrated to have a time slice every 0.05 years. The strike grid of the local volatility surface has 200 points, spanned uniformly over 3 standard deviations from the ATMF strike value. The maximum simulation time step is set at 0.01 years for both calibration and pricing.

We price a set of vanilla call options expiring at 10 years. Since we have the market implied volatility surface data $\Sigma(K, t)$, we can compare the Monte Carlo prices to analytical Black-Scholes vanilla call option prices implied by $\Sigma(K, t)$.

In Figure 2.1 we see that the convergence is achieved quickly with a relatively low number of paths at 1,000, where the pricing differences begin to be comparable in magnitude to the simulation Monte Carlo errors. The relatively low number of paths allow fast calibration.

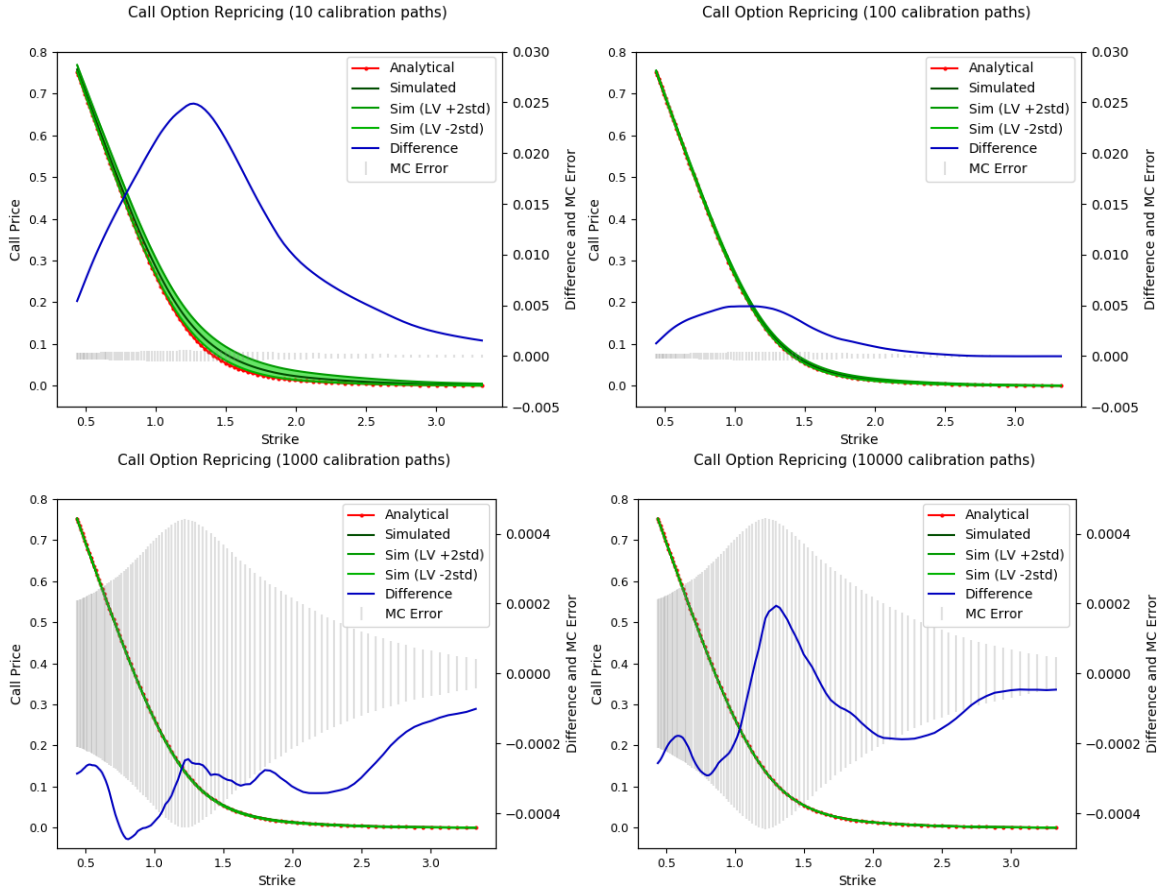


Figure 2.1: LV2SR: Repricing of vanilla call options with local volatility surfaces calibrated with varying number of paths. The pricing simulation is done with 100,000 paths to keep the simulation Monte Carlo error small. The pricing is done with the original calibrated surface as well as bumped down and bumped up surfaces according to Monte Carlo error introduced during the calibration. Comparison to Black-Scholes prices is made by observing the differences between the Monte Carlo and the analytical prices. One can observe that the pricing differences become comparable in magnitude to the simulation Monte Carlo errors at around 1,000 calibration paths.

For the convergence of the calibrated local volatility surface, two surfaces calibrated with 100,000 and 50,000 calibration paths respectively, were studied by looking at the difference between the surfaces in Figure 2.2. For the surfaces the x-axis represents the spot values of the underlier, the y-axis the time and z-axis the corresponding local volatility values. It can be seen that difference between the surfaces is roughly 1% of the magnitude of the local volatilities and the convergence of the surface is achieved for relatively small number of paths.

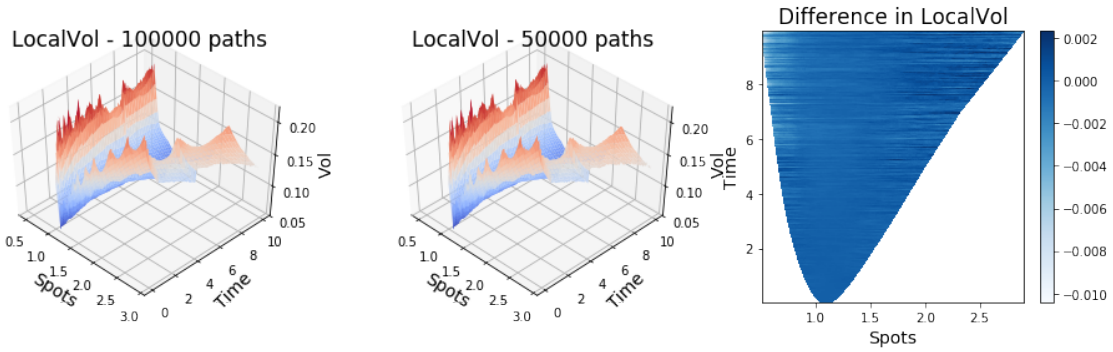


Figure 2.2: LV2SR: Calibrated local volatility surfaces with 100,000 calibration paths (left), 50,000 calibration paths (middle) and difference between the surfaces (right). The difference between the surfaces is roughly 1% of the magnitude of the local volatilities.

In order to study the effects of repricing, a local volatility surface calibrated with 100,000 paths was used for all subsequent tests presented in this section. The effect of number of repricing simulation paths for the given local volatility surface is shown in Figure 2.3 against the call option price and the corresponding MC error. As the MC error decreases with the number of simulation paths, between 1,000 and 100,000 paths the maximum absolute difference between the analytical and Monte Carlo priced call option values decreases from 9.1×10^{-4} to 5.1×10^{-4} .

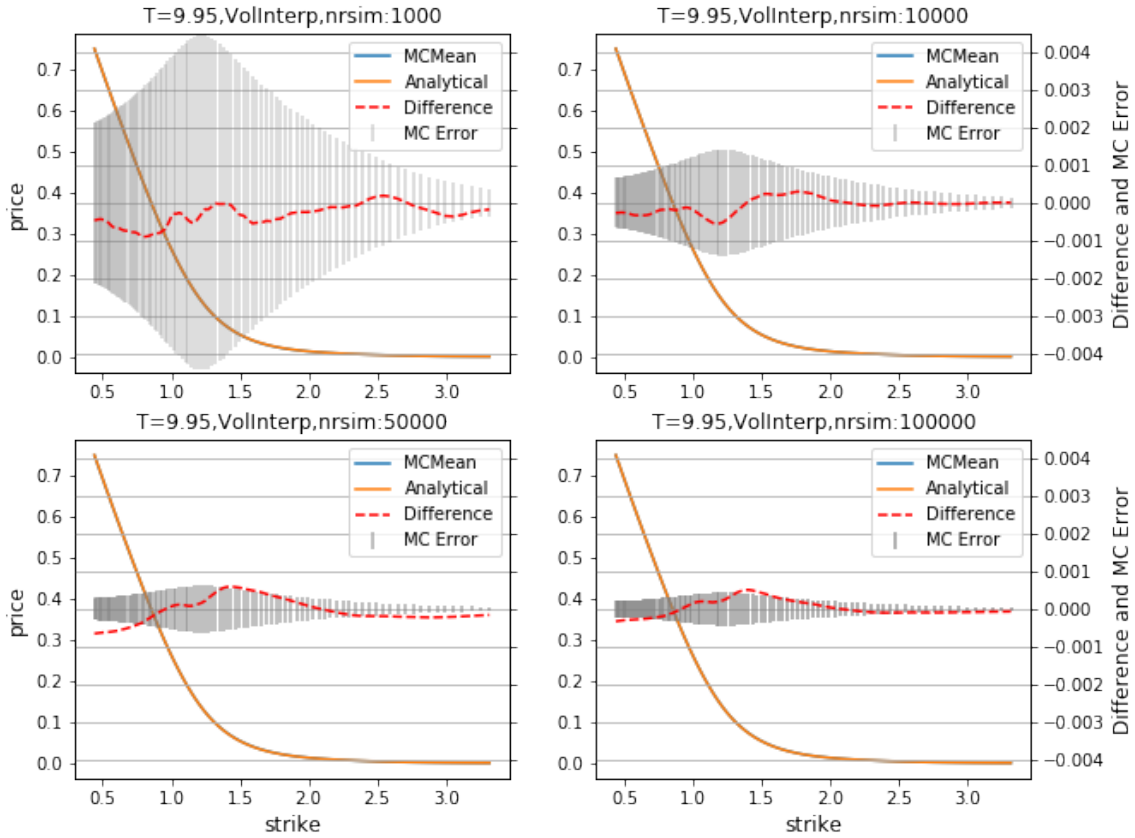


Figure 2.3: LV2SR: Repricing call options at 100 uniformly spaced strikes at maturity $T=9.95$ years, each with 100,000 (lower-right), 50,000 (lower-left), 10,000 (upper-right) and 1,000 (upper-left) MC simulation paths, using the local volatility surface calibrated with 100,000 MC simulation paths. The MC errors and the difference between the analytical and MC computed prices decreases with the number of simulation paths.

Furthermore, the calibrated local volatility surface was used to reprice the call options at multiple maturities and various strikes in the strike-grid to generate the so-called call price surface. The 100 maturities that are uniformly spaced between $T=0$ and 9.95 years, and 100 strikes per maturity were used to generate the call price surface shown in Figure 2.4a. The difference between the Monte Carlo repriced call option values and analytical Black-Scholes call option prices assuming constant interest rates and volatility is shown in Figure 2.4b, which is found to be less than 0.1% of the call option price.

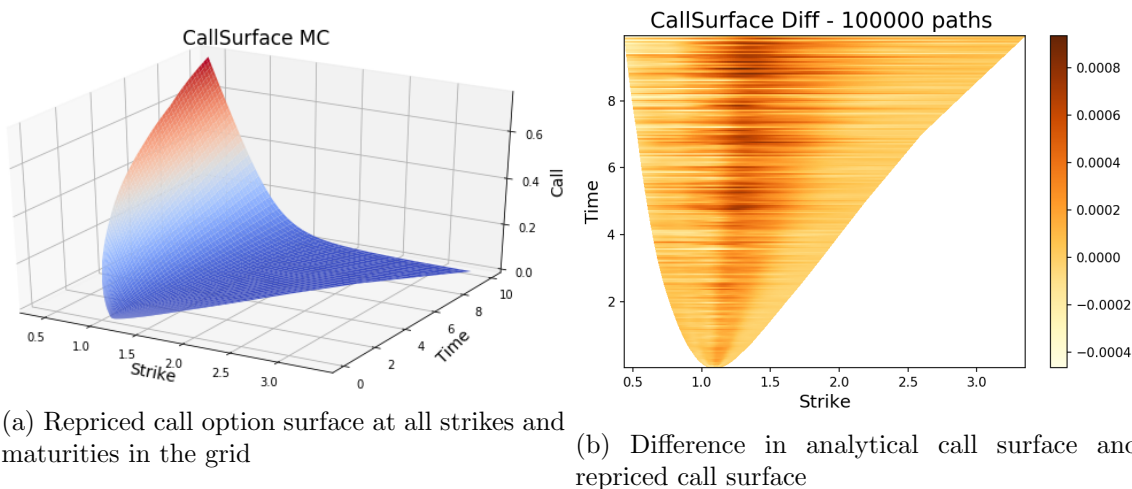


Figure 2.4: LV2SR: (a) Call options repriced at 100 uniformly spaced maturities between $T=0$ to 9.95 years and 100 strikes per maturity and (b) the difference between Monte Carlo and Black-Scholes analytical price.

Next, the market implied volatility and the implied volatility recovered from the Monte Carlo repriced options, by inverting the option price to evaluate Black-Scholes implied volatility, are compared in Figure 2.5 at maturity $T=9.95$. Additionally the implied volatility recovered from MC prices of out-of-the-money call and put options with ± 2 MC errors is presented.

It can be seen that recovered implied volatility is in good agreement with market implied volatility and the latter is found to be well within the ± 2 MC error bounds.

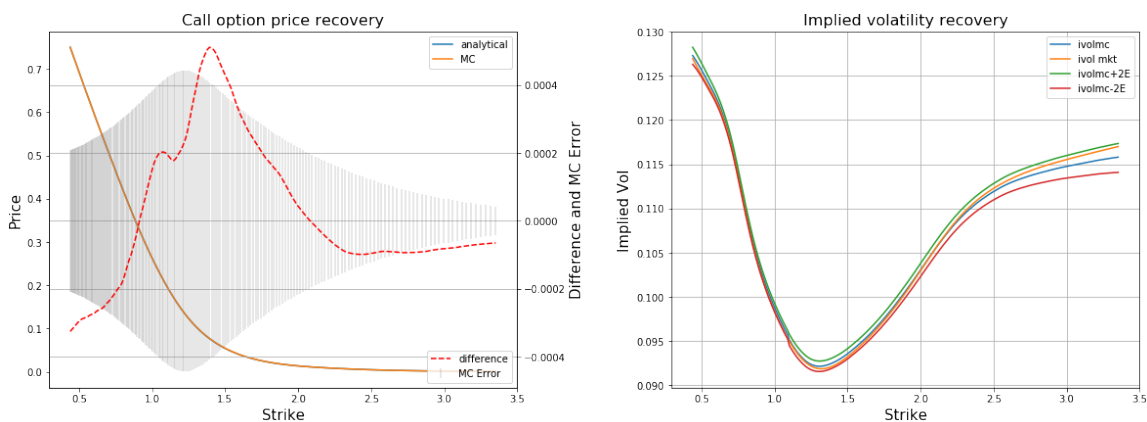


Figure 2.5: LV2SR: Difference between MC repriced vs analytical call options (left), implied volatility computed from repriced out-of-the-money call and put options vs market implied volatility at maturity(right) ($T=9.95$)

Finally, this procedure is repeated for all the maturities (time slices) in the repriced call surface, where the market and recovered implied volatility along with implied volatilities

corresponding to ± 2 MC pricing errors are shown for a few of the slices in Figure 2.6.

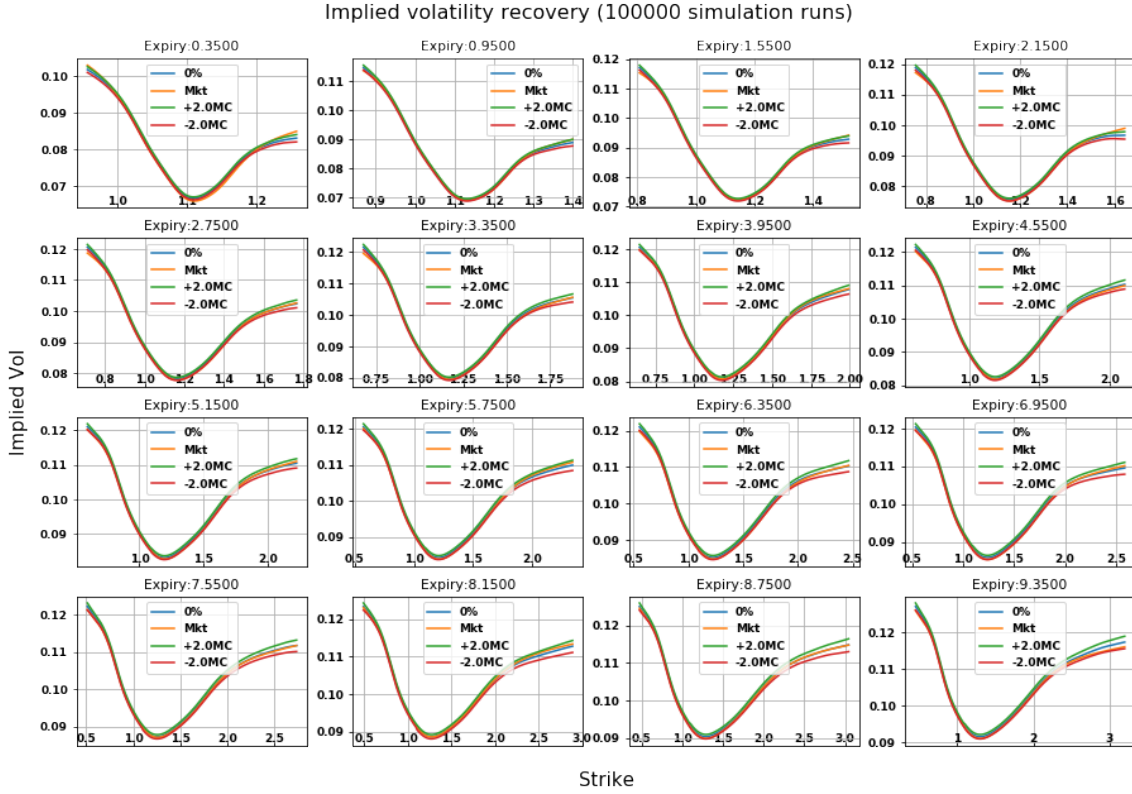


Figure 2.6: LV2SR: Implied volatility computed from repriced out-of-the-money call and put options vs the market implied volatility at various maturities

3 Stochastic Local Volatility Model (SLV2DR)

3.1 Setup

The standard local volatility model with deterministic interest rates (LV2DR)

$$dS_t = \left[r_t^d - r_t^f \right] S_t dt + \sigma_{LV}(S_t, t) S_t dW_t^{S(\text{DRN})} \quad (3.1)$$

can be extended to incorporate a stochastic nature in the diffusion term by replacing $\sigma_{LV}(S_t, t)$ with $L(S_t, t)\sqrt{U_t}$ where $L(S_t, t) > 0$ is the *leverage function* and (U_t) is the variance process. A common choice for (U_t) is the Cox-Ingersoll-Ross (CIR) process [8]. With this choice the SLV2DR SDE system is

$$\begin{aligned} dS_t &= \left[r_t^d - r_t^f \right] S_t dt + L(S_t, t) \sqrt{U_t} S_t dW_t^{S(\text{DRN})}, \\ dU_t &= \kappa_t(\theta_t - U_t) dt + \xi_t \sqrt{U_t} dW_t^{U(\text{DRN})}, \end{aligned} \quad (3.2)$$

with coefficient of correlation ρ_{SU} between the two Brownian drivers. This model can be seen as an augmentation of the Heston model [7], with $\kappa_t > 0$, $\theta_t > 0$, and $\xi_t > 0$ representing the

time-dependent mean reversion, long term variance, and vol-of-vol parameters. Together with the initial variance $U_0 > 0$, they form the set of Heston model parameters that will be calibrated to market data as we will describe below. The leverage function $L(S_t, t)$ is to be calibrated to recover market option prices.

The standard local volatility $\sigma_{LV}(S_t, t)$ is related to the leverage function $L(S_t, t)$ as [22]³

$$\sigma_{LV}(x, t)^2 = L(x, t)^2 \mathbf{E}^{\mathbb{Q}^{\text{DRN}}} [U_t | S_t = x]. \quad (3.3)$$

The main idea is to have the Heston parameters recover market vanilla option prices near ATMF strikes. The leverage function will then serve as a correction factor at the wings of the volatility surface.

3.2 Calibration of the Heston model parameters

In the limit where the calibration function is set to $L(S_t, t) = 1$, the stochastic local volatility model (3.2) reduces to the Heston model with time dependent coefficients,

$$\begin{aligned} dS_t &= [r_t^d - r_t^f] S_t dt + \sqrt{U_t} S_t dW_t^{S(\text{DRN})}, \\ dU_t &= \kappa_t (\theta_t - U_t) dt + \xi_t \sqrt{U_t} dW_t^{U(\text{DRN})}. \end{aligned} \quad (3.4)$$

Here we assume constant correlation between the two Brownian motions,

$$\left\langle dW^{S(\text{DRN})}, dW^{U(\text{DRN})} \right\rangle_t = \rho dt.$$

To improve calibration accuracy, one can trivially extend the model to admit time dependent correlation. However, we found that our simpler setup is sufficient for our purposes. The set of parameters we need to calibrate are the mean reversion $\kappa_t > 0$, the long term variance $\theta_t > 0$, the vol-of-vol $\xi_t > 0$, the coefficient of correlation ρ , and the initial variance $U_0 > 0$. Several methods have been studied in literature to calibrate these parameters, including an asymptotic approximation [24], or a semi-analytical approach computing the characteristic function and using control variates to regularize the numerical integration [25]. While these methods can be directly applied to our setup, we choose a simpler approach of calibrating the parameters using a PDE solver⁴. We note that this is not a binding choice, and one can use any reasonably fast solver to be repetitively called by the objective function of the optimizer that can accurately price under this model.

Inputs for calibration Our calibration routine expects the following quantities as input for Heston model with piecewise constant coefficients calibration:

- Spot FX rate S_0
- Market implied volatility $\Sigma(K, t)$ for FX rate

³We note that the expectation in [22] is given in domestic T -forward measure \mathbb{Q}^T , which is equal to domestic risk neutral measure \mathbb{Q}^{DRN} under deterministic rates.

⁴The PDE solver implements the two-dimensional backward Kolmogorov PDE for the Heston model with time dependent coefficients, using a standard finite difference alternating direction implicit (ADI) scheme [26].

- Market yield curves $P^d(0, t)$ and $P^f(0, t)$. Since the rates are deterministic, we have $r_t^i = f^i(0, t)$, $i = d, f$ where the instantaneous forward rate can be computed from the market yield curves, $f^i(0, t) \equiv -\frac{\partial \log P^i(0, t)}{\partial t}$.

Steps for calibration The calibration is done in a bootstrapping fashion. Let $t_i; i = 1, \dots, n$ be the increasing sequence of (positive) times where we will perform the calibration. At each calibration step, we make sure the Feller condition $2\kappa_{t_i}\theta_{t_i} > \xi_{t_i}^2$ is satisfied [8, 27] in order to keep the variance (U_t) strictly positive, by adding a suitable penalty function to the objective function. We choose the simplex algorithm [28] to do the optimization. The parameters κ_t , θ_t , and ξ_t are assumed to be piecewise constant.

1. For all calibration time slices t_i and predetermined ranges of strikes K_j , compute a grid of market vanilla call or put option prices using the input market implied volatility $\Sigma(K_j, t_i)$.
2. Using the PDE pricer, solve for all five parameters κ_{t_1} , θ_{t_1} , ξ_{t_1} , ρ , and U_0 to match the market vanilla option prices expiring at t_1 , generated in the first step.
3. For the subsequent slices $t_i; i > 1$, using the results of the previous slices in the PDE pricer, solve for the three parameters κ_{t_i} , θ_{t_i} , and ξ_{t_i} to match the market vanilla option prices expiring at t_i .

Since our primary goal of calibrating the Heston model parameters is to recover market quotes around ATMF strikes, we choose the strike grid to cover a narrower range than in the subsequent calibration routine of the leverage function.

3.3 Calibration and Simulation Tests for the Heston model

The strike grid is chosen uniformly over 1 standard deviation away in both directions from the ATMF strike value for each slice. The calibrated Heston parameters obtained by the procedure outlined above are visualized in Figure 3.1.

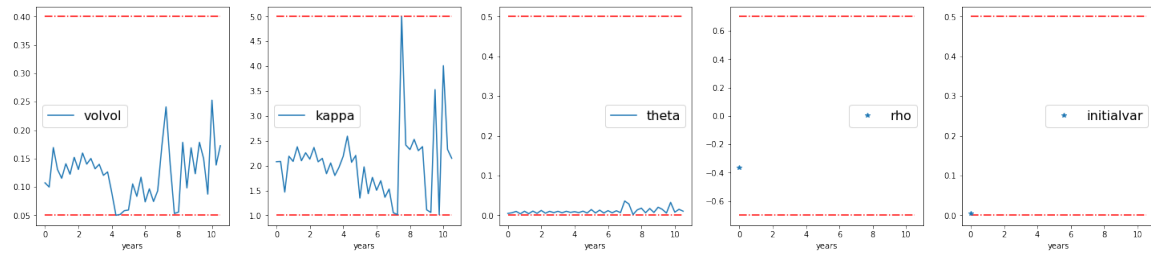


Figure 3.1: Heston model: Time-Series of calibrated model parameters

The figure shows that the calibrated parameters are mostly within bounds typically encountered in practice. These parameters will be used in calibration of the leverage function for the stochastic local volatility model as outlined in the subsequent section. We test the validity of the calibrated Heston parameters, which corresponds to the SLV2DR model (3.2) with the leverage function $L(S_t, t)$ set to 1.0, by pricing vanilla options by simulation. Thus

we can examine these call option prices close to ATMF. The repriced call option values at maturity and the implied volatilities computed from repriced out-of-the-money call and put options are shown in Figure 3.2. It can be seen that the recovered call option prices as well as the implied volatilities are near market quoted prices and implied volatilities for strikes within the calibration region.

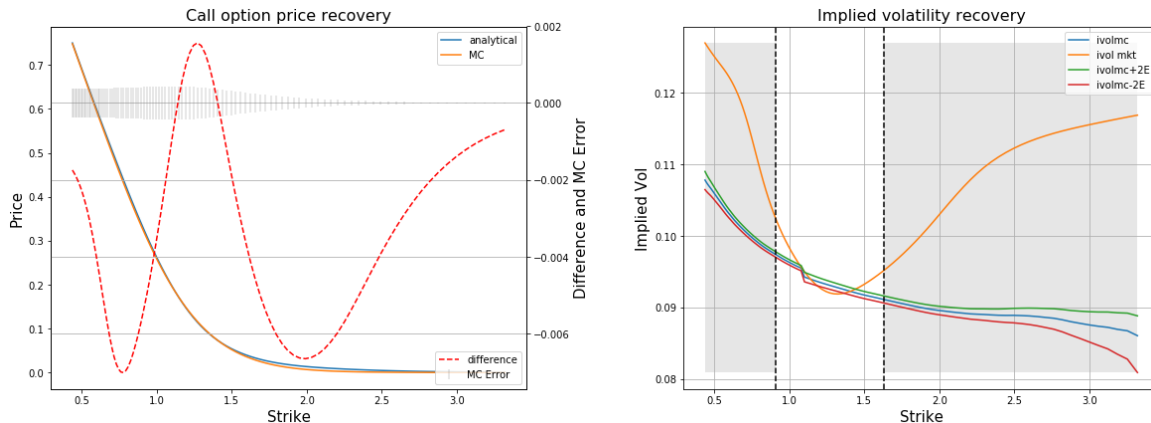


Figure 3.2: Heston model: Difference in repriced vs analytical call options (left), implied volatility from repriced out-of-the-money call and put options vs market implied volatility at maturity(right) (T=9.95). The dashed lines indicate the calibration range.

We perform an implied volatility recovery test at various maturities by inverting the simulated Heston model prices to compute the Black-Scholes implied volatility. We compare this with the market implied volatility in Figure 3.3. The recovered implied volatility is found to be in good agreement with the market implied volatility for strikes within the calibration range, as indicated in the plot.

3.4 Calibration of the Leverage Function

There are various methods proposed in the literature to estimate the conditional expectation in (3.3). The standard approach involves solving a forward Kolmogorov PDE that describes the forward evolution of the probability density function of the underlier; e.g. the FX rate. Here we introduce two methods that can be implemented by Monte Carlo simulation. The Monte Carlo approach we introduce here can be used with problems of higher dimension; such as a multi-factor stochastic volatility model, or the SLV2SR model that we will demonstrate in Section 4, where standard PDE methods cannot be applied due to curse of dimensionality.

3.4.1 Binning Approach

Suppose we simulate N Monte Carlo paths (S^i, U^i) , $i = 0, \dots, N - 1$ up to time t . At time t , we sort these paths by S^i . Let us denote by (\hat{S}^i, \hat{U}^i) the sorted pairs. We divide these

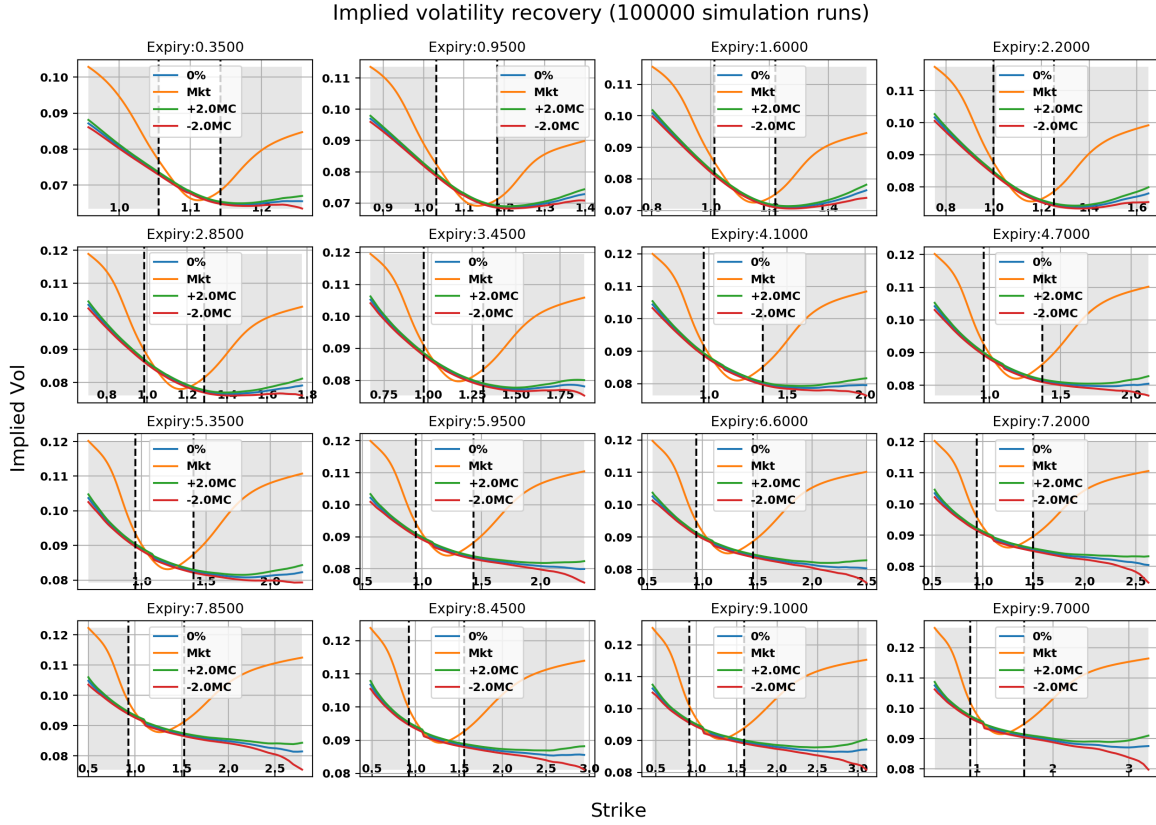


Figure 3.3: Heston model: Implied volatility computed from repriced out-of-the-money call and put options vs the market implied volatility at various maturities. The dashed lines indicate the calibration range at each maturity.

pairs into M bins, each bin containing N/M pairs. We compute the bin averages as

$$\tilde{S}^j = \frac{M}{N} \sum_{k=0}^{\frac{N}{M}-1} \hat{S}_{\frac{N}{M}j+k}^j,$$

$$\tilde{U}^j = \frac{M}{N} \sum_{k=0}^{\frac{N}{M}-1} \hat{U}_{\frac{N}{M}j+k}^j.$$

with $j = 0, \dots, M - 1$. By computing the interpolation function for \tilde{S}^j against \tilde{U}^j , we can estimate the expectation in (3.3) for a given S_t .

3.4.2 Regression Approach

The idea is to linearly regress the variance values U_t against basis functions $f^n(\cdot)$ of the underlying spot rate values S_t . After simulating N Monte Carlo paths (S^i, U^i) , $i = 0, \dots, N -$

1 up to time t , we compute the regression coefficients a_n by solving the least squares problem

$$\hat{U}_t = \sum_n a_n f^n(S_t). \quad (3.5)$$

Standard monomials or orthogonal polynomials with appropriate limits can be used as basis functions. For example, if we use a constant term and the first two orders of monomials, we need to solve

$$\hat{U}_t = a_1 + a_2 S_t + a_3 S_t^2. \quad (3.6)$$

After computing the regression coefficients a_n , we can use this regression equation to evaluate the expected value of U_t for a given S_t , which gives us the conditional expectation in (3.3).

Inputs for calibration Our calibration routine expects the following quantities as input for leverage function calibration:

- Spot FX rate S_0
- Market implied volatility $\Sigma(K, t)$ for FX rate
- Market yield curves $P^d(0, t)$ and $P^f(0, t)$. Since the rates are deterministic, we have $r_t^i = f^i(0, t)$, $i = d, f$ where the instantaneous forward rate can be computed from the market yield curves, $f^i(0, t) \equiv -\frac{\partial \log P^i(0, t)}{\partial t}$.
- Heston model parameters $\kappa_t, \theta_t, \xi_t, \rho$, and U_0 calibrated to market vanilla option prices as in Section 3.2. The strike grid is chosen to be near ATMF strikes. In particular it should be smaller than (e.g. one third of) the local volatility strike range.

Steps for calibration The calibration is done in a bootstrapping fashion. Let $t_i; i = 1, \dots, n$ be the increasing sequence of (positive) times where we will perform the calibration. After computing the leverage function values for a time slice t_j , the values are used during the subsequent simulations to estimate the leverage function values at the next time slice.

1. Using the market implied volatility $\Sigma(K, t)$, generate a vanilla call option price surface $C(K, t)$ interpolator or a total implied variance surface $w(y, t)$ interpolator. The interpolator must be able to evaluate the partial derivatives appearing in the local volatility expressions.
2. Compute the deterministic local volatility $\sigma_{LV}(K, t)$ by (2.17) or (2.19) for all calibration time slices t_i and predetermined ranges of strikes.
3. Simulate the SDE system (3.2) up to time t_j . Compute the Monte Carlo estimate for the conditional expectation appearing in (3.3) for the same range of strikes from the previous step by using one of the approaches described in the previous sections. Use this equation to obtain the leverage function values $L(K, t)$. These leverage function values will be used during subsequent simulation steps from time t_j to time t_{j+1} .

The strike grid can be chosen to be uniform across all calibration time slices. In this approach, however, the strike grid needs to be sufficiently large to cover attainable values of the FX rate at long expiries. This in turn would result in unreliable local volatility values at short expiries and strikes in the far wings. To overcome this problem, we suggest using a more adequate strike grid at each calibration time slice, e.g. one that spans a predetermined number of standard deviations away from the ATMF strike value. Another plausible approach is choosing the strike grid to cover the range of strikes that the implied volatility surface is calibrated to, if this information is available. For the Heston parameters calibration, we suggest using a similar grid with a smaller range, e.g. one third of the local volatility grid range.

3.5 Calibration and Simulation Tests for the Leverage Function

In order to test the calibration convergence, the differences between the calibrated leverage functions with 100,000 and 50,000 MC paths are visualized in Figure 3.4 across the strike grid at various time slices. As the figure shows, the differences are minor, indicating the achievement of convergence.

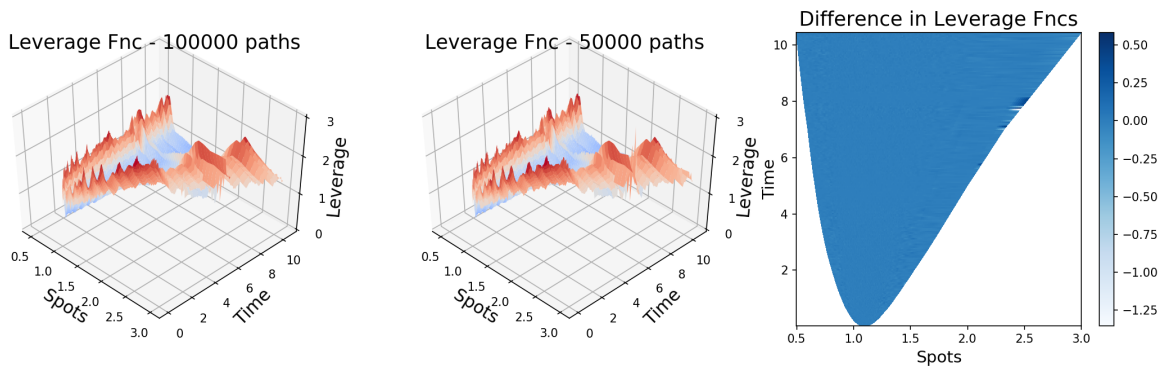


Figure 3.4: SLV2DR: Difference in leverage function with respect to the calibration Monte Carlo paths

The leverage function calibrated with 100,000 MC paths was used for all subsequent tests including repricing and implied volatility recovery. The call option was repriced for strikes at maturity with the above leverage function, with various number of simulation MC paths as shown in Figure 3.5. As the MC error decreases with the number of simulation paths, between 1,000 and 100,000 paths the maximum absolute difference between the analytical and Monte Carlo priced call option values decreases from 0.0128 to 0.0015.

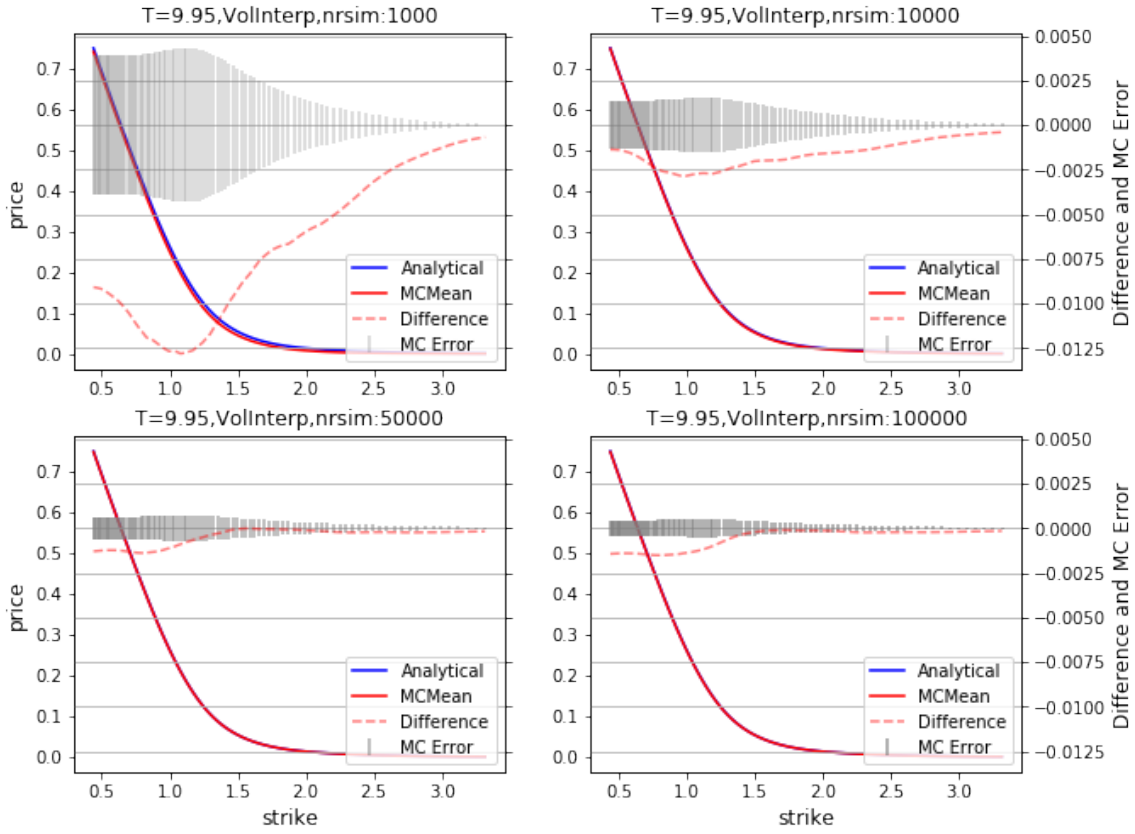


Figure 3.5: SLV2DR: Repricing the call options with different simulation Monte Carlo paths using leverage function calibrated with 100,000 Monte Carlo paths

We perform a simulation to reprice vanilla call options across the strike grid at various maturities to obtain the so called call surface. The difference between the analytical call price surface implied by $\Sigma(K, t)$ and repriced surface using 100,000 MC paths at each strike and maturity is visualized in Figure 3.6. The differences appear to be small compared to option prices.

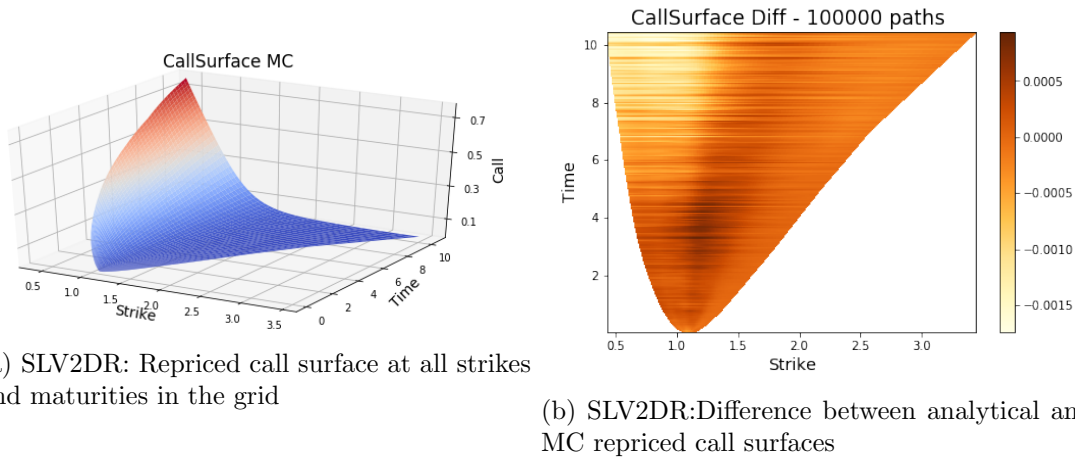


Figure 3.6: SLV2DR: Call options repriced at all strikes and maturities and the difference from BS analytical price

The implied volatility for the repriced out-of-the-money call and put options at maturity was obtained by inverting option values with Black-Scholes formula. The recovered implied volatility is compared to market implied volatility as shown in Figure 3.7. This is also performed for option prices obtained by bumping them by ± 2 MC errors. The market implied volatility and the recovered implied volatility are found to be in good agreement with each other.

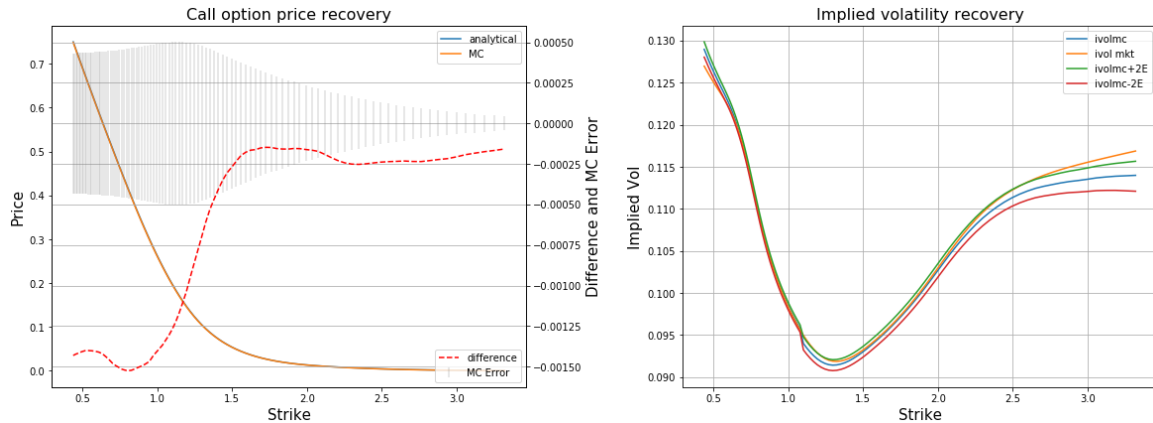


Figure 3.7: SLV2DR: Difference in repriced vs analytical call options (left), implied volatility from repriced out-of-the-money call and put option vs market implied volatility at maturity (right) ($T=9.95$)

Finally, the same procedure of recovering implied volatility with the repriced out-of-the-money call and put option values, is repeated at multiple maturities and strikes for different time slices, as shown in Figure 3.8, which is also found to be in good agreement with the given market implied volatility. We note that our implied volatility recovery results are consistent with those demonstrated in [17] where the authors calibrate the stochastic local

volatility model by solving a two-dimensional forward Kolmogorov PDE.

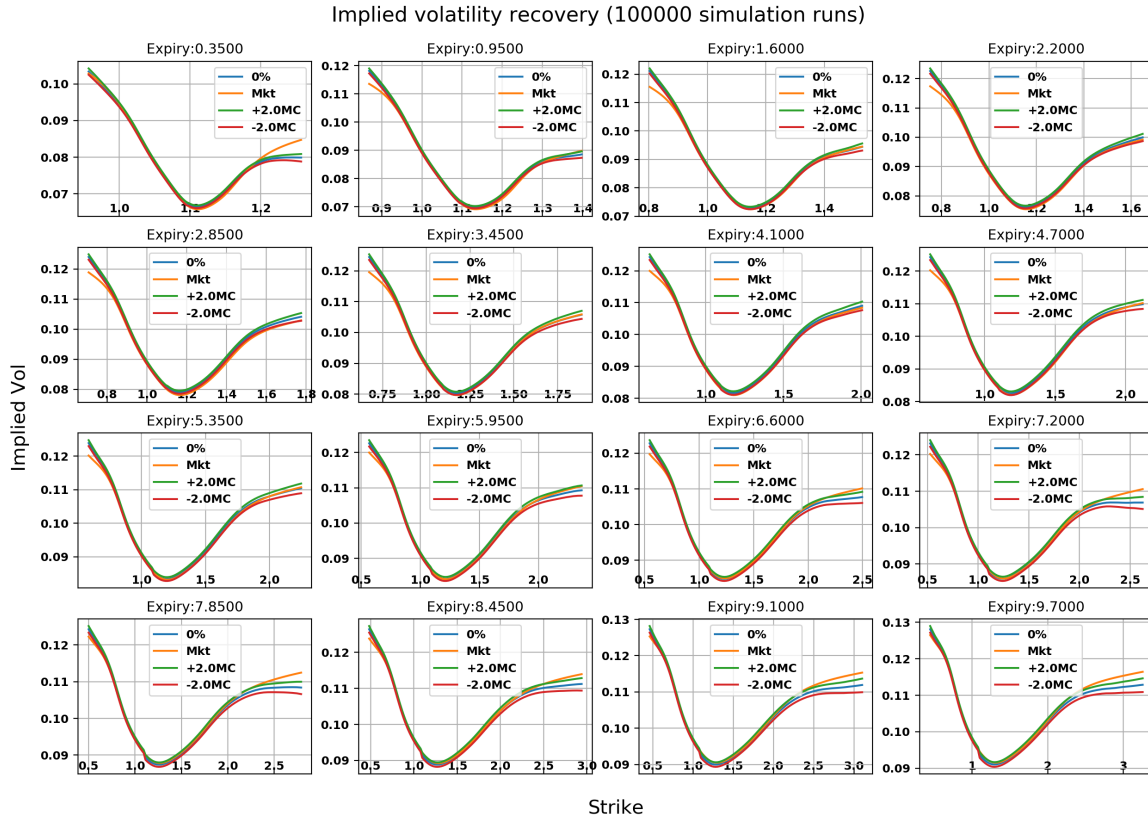


Figure 3.8: SLV2DR: Implied volatility computed from repriced out-of-the-money call and put options vs the market implied volatility at various maturities

We have observed in Figures 3.2 and 3.3 that the pure Heston model recovered market quotes near ATM strikes. Comparison of these to Figures 3.5 and 3.8 shows us the improvement of the full stochastic local volatility model over the Heston model at all strikes. In particular, we see that the pricing error was reduced by a factor of 4, and the market implied volatilities are recovered along a greater range.

4 Stochastic Local Volatility Model with Stochastic Interest Rates (SLV2SR)

4.1 Setup / Model Definition

This model can be seen as an extension to both local volatility model with stochastic interest rates (LV2SR) and stochastic local volatility model with deterministic interest rates (SLV2DR). Considering an FX rate process with stochastic local volatility and stochastic interest rates, the SLV2SR SDE system can be written in the domestic risk neutral measure

\mathbb{Q}^{DRN} as

$$\begin{aligned}
dS_t &= \left[r_t^d - r_t^f \right] S_t dt + L(S_t, t) \sqrt{U_t} S_t dW_t^{S(\text{DRN})}, \\
dU_t &= \kappa_t (\theta_t - U_t) dt + \xi_t \sqrt{U_t} dW_t^{U(\text{DRN})}, \\
r_t^d &= x_t^d + \phi_t^d, \\
dx_t^d &= -a_t^d x_t^d dt + \sigma_t^d dW_t^{d(\text{DRN})}, \\
r_t^f &= x_t^f + \phi_t^f, \\
dx_t^f &= \left[-a_t^f x_t^f - \rho_{Sf} \sigma_t^f L(S_t, t) \sqrt{U_t} \right] dt + \sigma_t^f dW_t^{f(\text{DRN})},
\end{aligned} \tag{4.1}$$

with coefficients of correlation ρ_{SU} (FX rate/FX variance), ρ_{Sd} (FX rate/domestic interest rate), ρ_{Sf} (FX rate/foreign interest rate), ρ_{Ud} (FX variance/domestic interest rate), ρ_{Uf} (FX variance/foreign interest rate), and ρ_{df} (domestic interest rate/foreign interest rate) between the respective Brownian motions.

One can relate the standard local volatility $\sigma_{\text{LV}}(S_t, t)$ to the leverage function $L(S_t, t)$ by [22]

$$\sigma_{\text{LV}}(x, t)^2 = L(x, t)^2 \mathbf{E}^{\mathbb{Q}^T} [U_t \mid S_t = x]. \tag{4.2}$$

Since our calibration algorithm presented in the next section demands Monte Carlo estimation of the above expectation in the domestic T -forward measure \mathbb{Q}^T , we need to formulate the SDE system in this measure. The T -forward measure SDEs for the exchange rate, domestic short rate and domestic short rate are derived the same way as in Section 2.1.2. The remaining computation is for the stochastic variance SDE, which we present here.

Let ρ_{Ud} is coefficient of correlation between the Brownian motions $(W_t^{U(\text{DRN})})$ and $(W_t^{d(\text{DRN})})$, that is $d\langle W_t^{U(\text{DRN})}, W_t^{d(\text{DRN})} \rangle_t = \rho_{Ud} dt$. The domestic risk neutral measure \mathbb{Q}^{DRN} to domestic T -forward measure \mathbb{Q}^T transformation is characterized by (2.12), Following Lemma A.1, the variance process (4.1) evolves in domestic T -forward measure \mathbb{Q}^T as

$$dU_t = \left[\kappa_t (\theta_t - U_t) - \rho_{Ud} b^d(t, T) \sigma_t^d \xi_t \sqrt{U_t} \right] dt + \xi_t \sqrt{U_t} dW_t^{U(T)}. \tag{4.3}$$

Collecting everything,

$$\begin{aligned}
dS_t &= \left[r_t^d - r_t^f - \rho_{Sd} b^d(t, T) \sigma_t^d L(S_t, t) \sqrt{U_t} \right] S_t dt + L(S_t, t) \sqrt{U_t} S_t dW_t^{S(T)}, \\
dU_t &= \left[\kappa_t (\theta_t - U_t) - \rho_{Ud} b^d(t, T) \sigma_t^d \xi_t \sqrt{U_t} \right] dt + \xi_t \sqrt{U_t} dW_t^{U(T)}, \\
r_t^d &= x_t^d + \phi_t^d, \\
dx_t^d &= \left[-a_t^d x_t^d - b^d(t, T) (\sigma_t^d)^2 \right] dt + \sigma_t^d dW_t^{d(T)}, \\
r_t^f &= x_t^f + \phi_t^f, \\
dx_t^f &= \left[-a_t^f x_t^f - \rho_{Sf} \sigma_t^f L(S_t, t) \sqrt{U_t} - \rho_{df} b^d(t, T) \sigma_t^d \sigma_t^f \right] dt + \sigma_t^f dW_t^{f(T)}
\end{aligned} \tag{4.4}$$

describe the evolutions of the exchange rate, exchange rate variance, domestic short rate, and foreign short rate processes under the domestic T -forward measure \mathbb{Q}^T .

4.2 Calibration of the Leverage Function

The standard forward Kolmogorov PDE approach to solve the conditional expectation in (4.2) suffers from the curse of dimensionality, as this is now a 4D problem. Similarly, the binning approach utilized in Section 3.4.1 for the model with deterministic interest rates can not be applied directly, at least without any simplifying assumptions, as the sorting of the underliers becomes nontrivial.

As in the case of stochastic local volatility model with deterministic interest rates, the calibration is done in a bootstrapping fashion, after computing the leverage function values for a time slice t , the values are used during the subsequent simulation to estimate the leverage function values at the next time slice. The Heston model parameters are assumed to be calibrated to match an appropriate subset of market data.

The idea is to linearly regress the variance values U_t against basis functions $f^n(\cdot)$ of the underlying spot rate values S_t , and the two interest rate values r_t^d and r_t^f . After simulating N Monte Carlo paths $(S^i, r^{d,i}, r^{f,i}, U^i)$, $i = 0, \dots, N - 1$ up to time t , we compute the regression coefficients a_n by solving the least squares problem

$$\hat{U}_t = \sum_n a_n f^n(S_t, r_t^d, r_t^f). \quad (4.5)$$

Standard monomials or orthogonal polynomials can be used as basis functions. For example, if we use a constant term and the first two orders of monomials for all underliers, we need to solve

$$\hat{U}_t = a_1 + a_2 S_t + a_3 S_t^2 + a_4 x_t^d + a_5 x_t^{d^2} + a_6 x_t^f + a_7 x_t^{f^2}. \quad (4.6)$$

Note that in this example we used the x_t^d and x_t^f as the basis functions instead of the short rates r_t^d and r_t^f ; the deterministic parts ϕ_t^d and ϕ_t^f of the latter can be absorbed into other coefficients. After computing the regression coefficients a_n , we can use this regression equation to evaluate the expected value of U_t for given S_t , r_t^d , and r_t^f , which gives us the conditional expectation in (4.2).

Inputs for calibration Our calibration routine expects the following quantities as input for leverage function calibration:

- Spot FX rate S_0
- For both domestic and foreign rates, G1++ model parameters mean reversion, volatility and shift function calibrated to market data⁵
- Coefficients of correlation between all underlying assets: the FX rate, its variance, the domestic and foreign short rates
- Local volatility (with stochastic rates) surface data, as calibrated in Section 2.2
- Heston model (with deterministic rates) parameters, as calibrated in Section 3.2

⁵See [23] for example calibration methods for both constant and time dependent cases.

Steps for calibration In our framework, we calibrate the leverage function surface time slice by time slice, in a bootstrapping fashion. Let $t_i; i = 0, \dots, n$ be the increasing sequence of times where we will perform the calibration. The first time slice is $t_0 = 0$.

1. For t_0 , (4.2) simplifies to $\sigma_{LV}(K, 0)^2 = L(K, 0)^2 U_0$, where $\sigma_{LV}(K, t)^2$ is the local volatility with stochastic rates. Use this equation to evaluate the leverage function for the t_0 slice for a predetermined range of strikes.
2. For each of the subsequent positive time slices $t_j, j \geq 1$, simulate the SDE system (4.4) up to time t_j . Compute the Monte Carlo estimate for the expectation appearing in (4.2) for a predetermined range of strikes. Use this equation to obtain the leverage function values. These leverage function values will be used during subsequent simulation steps from time t_j to time t_{j+1} .

The strike grid for the leverage function $L(K, t)$ is chosen to be the same as the strike grid for the local volatility $\sigma_{LV}(K, t)$ to avoid any inaccuracy introduced by interpolation.

4.3 Calibration and Simulation Tests

The G1++ model parameters we use as input are summarized in Table 2.1. The coefficients of correlation are given by $\rho_{Sd} = 0.166, \rho_{Sf} = 0.551, \rho_{df} = 0.161$.

In order to calibrate the SLV2SR model, the Heston model parameters computed during the SLV2SR model calibration and the local volatility function calibrated for the LV2SR model with 100,000 MC paths were used. The procedure outlined above was followed in order to iteratively compute the leverage function for each time slice. In order to evaluate the expectation appearing in (4.2), 100,000 MC paths followed by regression with monomials of order 2 for each of the underlying regressors (S_t, x_t^d, x_t^f) along with the constant coefficient a_1 as in (4.6) were used. The results for the calibration and repricing tests are presented below.

The effect of number of repricing simulation paths for the given local volatility surface is shown in Figure 4.1 against the call option price and the corresponding MC error. As the MC error decreases with the number of simulation paths, between 1,000 and 100,000 paths the maximum absolute difference between the analytical and Monte Carlo priced call option values decreases from 0.00437 to 0.00146.

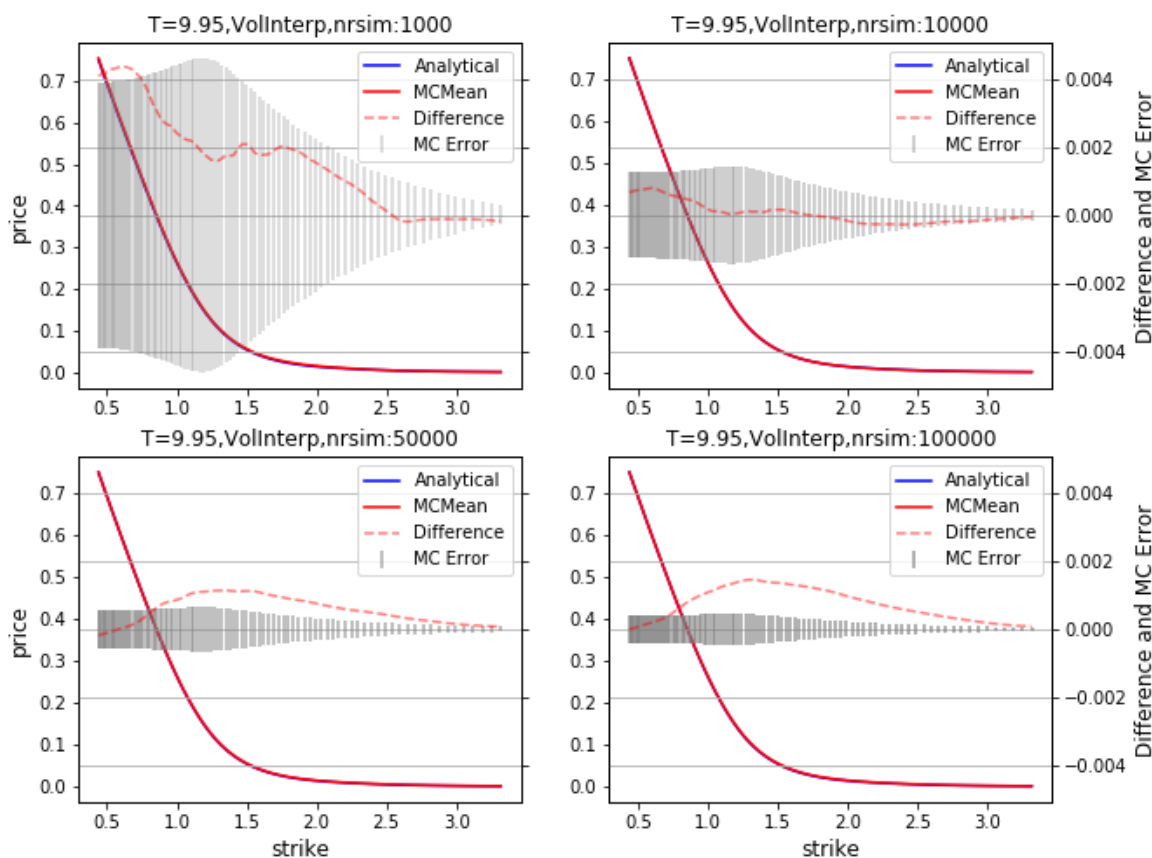


Figure 4.1: SLV2SR: Repricing call options with various simulation Monte Carlo paths using leverage function calibrated for SLV2DR with 100,000 MC paths and multi-regression approach with 100,000 MC paths.

Furthermore, the local volatility surface was used to reprice call options at multiple maturities and various strikes in the strike-grid to generate the so-called call price surface. 100 maturities uniformly spaced between $T=0$ and 9.95 years, and 100 strikes per maturity were used to generate the call price surface shown in Figure 4.2a. The difference between the Monte Carlo repriced call option values and analytical Black-Scholes call option prices, implied by $\Sigma(K, t)$, assuming constant interest rate and volatility is shown in Figure 4.2b, which is found to be less than 1% of the call option price.

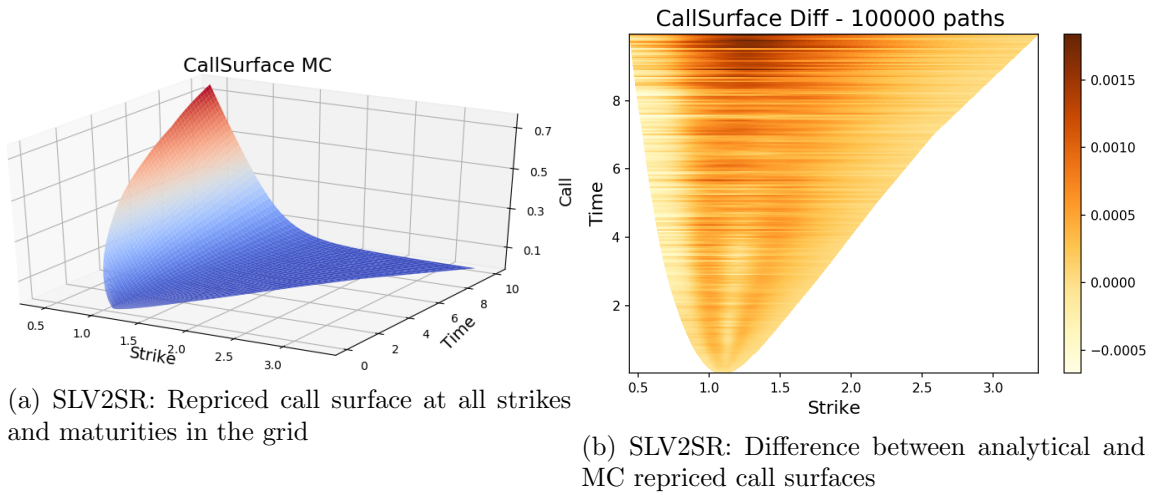


Figure 4.2: SLV2SR: Call options repriced at all strikes and maturities and the difference from BS analytical price

Next, the market implied volatility and the implied volatility recovered from the Monte Carlo repriced out-of-the-money call and put options, by inverting the Black-Scholes formula, are compared in Figure 4.3 at maturity $T=9.95$. In addition the implied volatility recovered from MC prices ± 4 MC errors are presented. It can be seen that recovered implied volatility is in good agreement with market implied volatility.

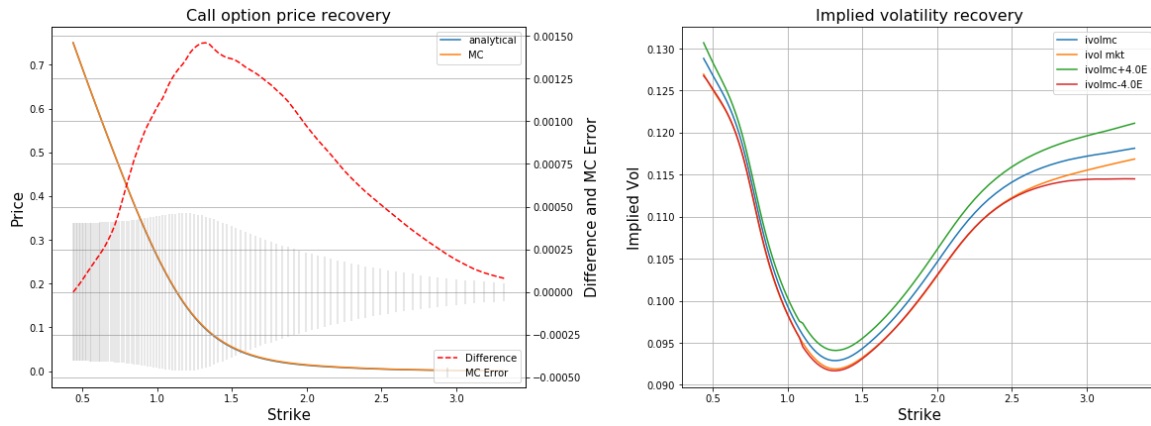


Figure 4.3: SLV2SR: Difference between MC repriced and analytical call options (left), implied volatility from repriced out-of-the-money call and put options vs market implied volatility at maturity(right) ($T=9.95$)

Finally, this procedure is repeated for all the maturities (time slices) in the repriced call surface, where the market and recovered implied volatility along with implied volatilities corresponding to ± 4 MC pricing errors for a few of the slices are shown in Figure 4.4.

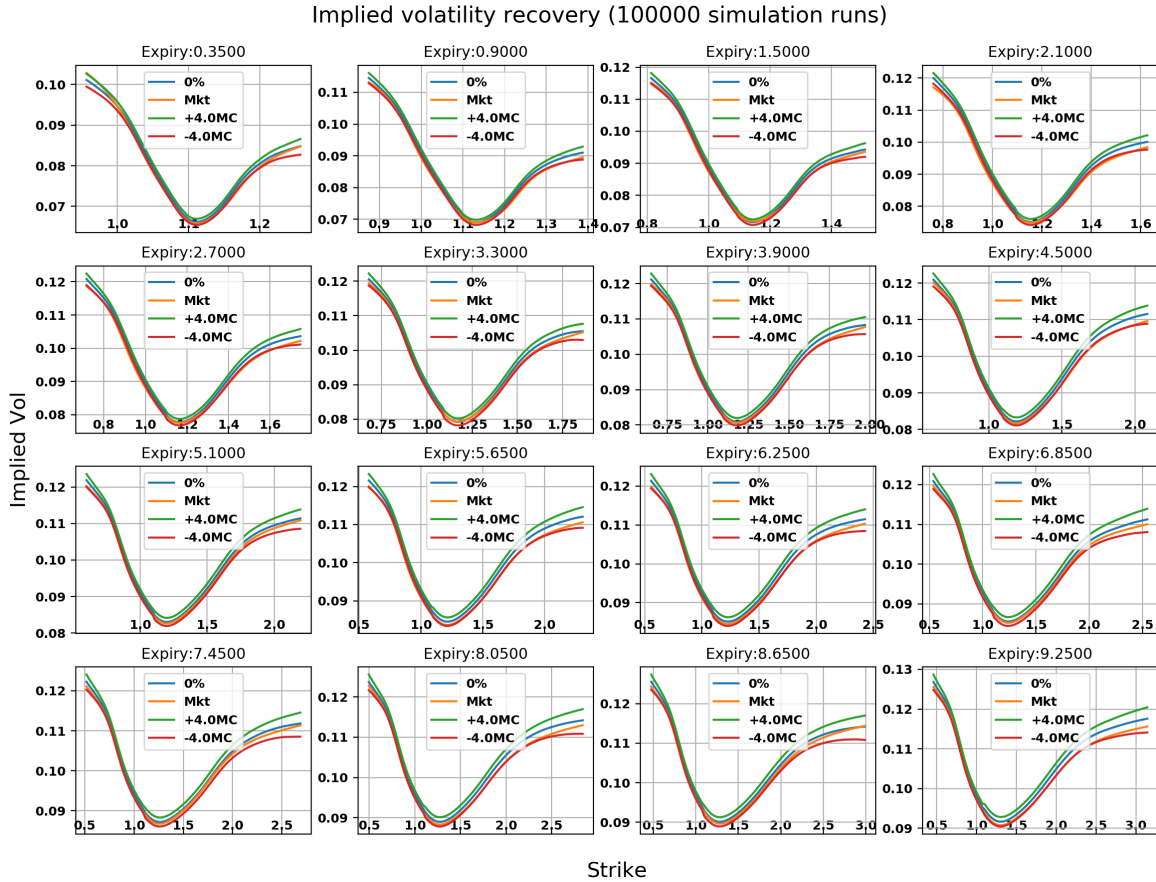


Figure 4.4: SLV2SR: Implied volatility computed from repriced out-of-the-money call and put option vs the market implied volatility at various maturities

5 Further Studies and Conclusions

We studied the convergence and the vanilla option repricing accuracy of the LV2SR, SLV2DR and SLV2SR models calibrated with the proposed algorithms. While all three models perform decently with recovering market implied volatilities, we found that as the models get more complex, e.g. when they have higher number of parameters, one needs to increase the number of simulation paths to maintain the accuracy, which in turn results in increased calibration time.

We are now in a position to assess the pricing inaccuracies of the three main models (LV2SR, SLV2DR and SLV2SR) we considered in this paper. To gain a more comprehensive perspective, we also simulate the standard local volatility model with two interest rates LV2DR (3.1) where the local volatility is computed from market implied volatility by (2.19). For the LV2DR model, Figure 5.1 demonstrates the convergence of the Monte Carlo price with respect to the number of simulated paths, and Figure 5.2 shows the Monte Carlo simulated call price surface and its difference from the analytical call price surface implied by market data.

With fixed number of calibration and simulation paths, we observe that the SLV2DR

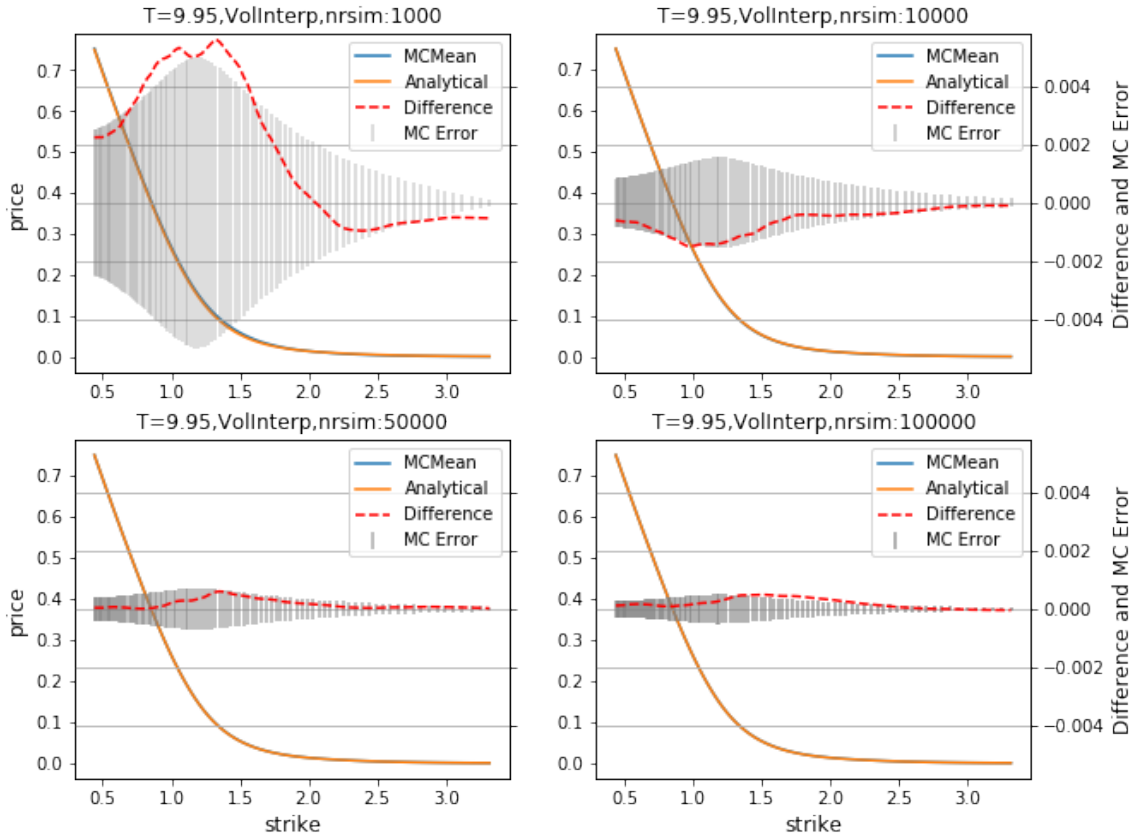


Figure 5.1: LV2DR: Repricing call options at 100 uniformly spaced strikes at maturity $T=9.95$ years, each with 100,000 (lower-right), 50,000 (lower-left), 10,000 (upper-right) and 1,000 (upper-left) MC simulation paths, using the local volatility surface calibrated with 100,000 MC simulation paths. The MC errors and the difference between the analytical and MC computed prices decreases with the number of simulation paths.

model (see Figures 3.5, 3.6, 3.7) reprices market quotes slightly more accurately than the SLV2SR model (see Figures 4.1, 4.2, 4.3). In the meantime, we see that our simplest model, LV2SR (see Figures 2.3, 2.4, 2.5) gives the smallest repricing errors among the three models. In the meantime, we observe that the accuracy of LV2SR calibration is comparable to, and arguably slightly better than, that of LV2DR.

Recovering market quotes is clearly a property desired for any pricing model. In our case, the market quotes are vanilla option prices or an implied volatility surface. Yet the risk neutral price of a European vanilla option only depends on the terminal distribution of the underlier, which can be extracted from the implied volatility surface numerically. Thus, the three models we are considering are not strictly necessary to price vanilla options. What about instruments for which the payoff depends on the joint distribution of intermediate values of the underliers?

To study the pricing of path dependent options, we consider an up-and-out barrier call option with 5-year maturity struck at ATMF strike. Without the barrier feature, the

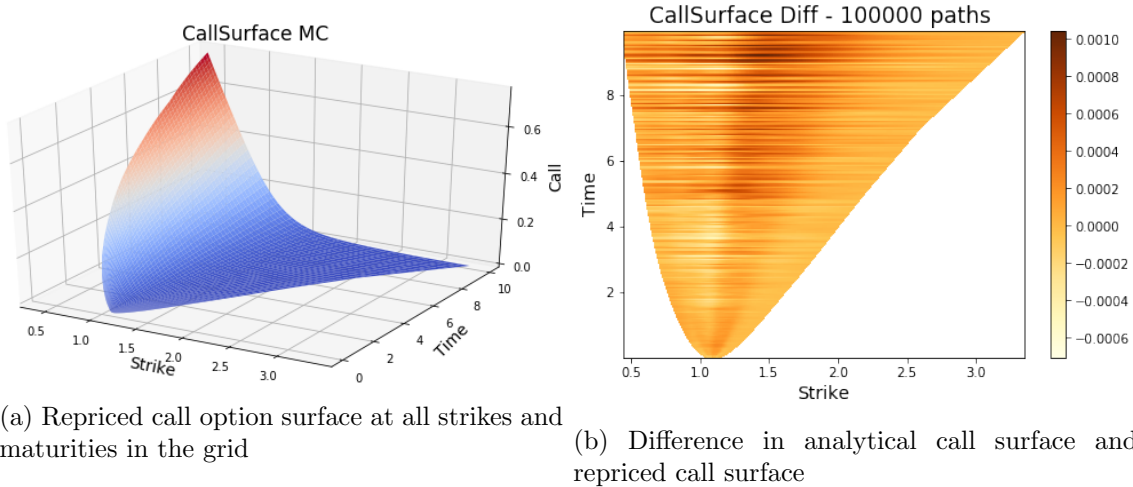


Figure 5.2: LV2DR: (a) Call options repriced at 100 uniformly spaced maturities between $T=0$ to 9.95 years and 100 strikes per maturity and (b) the difference between Monte Carlo and Black-Scholes analytical price.

instrument becomes a plain European vanilla call option, which has an analytical solution under the Black-Scholes model. The models under consideration price the option with valuation date 2020-04-30 and 100,000 simulation paths as in Table 5.1. We note that the

Table 5.1: Vanilla option pricing with various models. Prices and errors are given in basis points.

Model	Price ($\times 10^{-4}$)	Error ($\times 10^{-4}$)
Analytical (BS)	843.79	
LV2DR	845.53	2.93
LV2SR	846.33	2.86
SLV2DR	843.36	2.93
SLV2SR	846.51	2.89

analytical price is within the Monte Carlo error for all the four models, in consistency with the findings of the previous sections.

Now we turn the up-and-out barrier on and set the barrier position at 1.25 times the ATM strike. The barrier is active throughout the lifetime of the option. The standard Black-Scholes model admits an analytical solution for such barriers when the interest rates are constant [29]. The models under consideration price the option with the same valuation date and number of simulation paths as in Table 5.2. We find that the LV2DR and LV2SR model prices are within 2 Monte Carlo errors of the analytical price. However the SLV2DR and SLV2SR model prices are observed not to converge to the analytical BS price; i.e. their differences to the analytical price are larger in magnitude than the MC errors. This shows us the impact of stochastic volatility on the barrier option price.

While the stochasticity of the local volatility has a clear impact on the price of path dependent instruments, the stochasticity of interest rates have little effect under standard market conditions, e.g. when the interest rate volatilities are low. We expect this effect to

Table 5.2: Barrier option pricing with various models. Prices and errors are given in basis points.

Model	Price ($\times 10^{-4}$)	Error ($\times 10^{-4}$)
Analytical (BS)	285.55	
LV2DR	287.05	1.08
LV2SR	284.87	1.07
SLV2DR	299.00	1.14
SLV2SR	300.84	1.12

be more prominent in stressed environments with higher interest rate volatilities, which is what we study next.

Consider the stochastic rates extension of the Black Scholes model (BS2SR)

$$\begin{aligned}
dS_t &= \left[r_t^d - r_t^f \right] S_t dt + \sigma^S S_t dW_t^{S(\text{DRN})}, \\
dx_t^d &= -a_t^d x_t^d dt + \sigma_t^d dW_t^{d(\text{DRN})}, \quad r_t^d = x_t^d + \phi_t^d, \\
dx_t^f &= \left[-a_t^f x_t^f - \rho_{Sf} \sigma_t^f \sigma^S \right] dt + \sigma_t^f dW_t^{f(\text{DRN})}, \quad r_t^f = x_t^f + \phi_t^f.
\end{aligned} \tag{5.1}$$

This model can be seen as a special case of LV2SR with flat local volatility, which allows us to incorporate results from Section 2. Using (A.9) and Itô's lemma one can write the SDEs for the domestic and foreign zero coupon bonds in domestic risk neutral measure as

$$\begin{aligned}
\frac{dP^d(t, T)}{P^d(t, T)} &= r_t^d dt - \sigma_t^d b^d(t, T) dW_t^{d(\text{DRN})}, \\
\frac{dP^f(t, T)}{P^f(t, T)} &= \left[r_t^f + \rho_{Sf} \sigma^S \sigma_t^f b^f(t, T) \right] dt - \sigma_t^f b^f(t, T) dW_t^{f(\text{DRN})}.
\end{aligned} \tag{5.2}$$

Using (2.11) and Lemma A.1, these can be written in the domestic T -forward measure as

$$\begin{aligned}
\frac{dP^d(t, T)}{P^d(t, T)} &= \left[r_t^d + \left(\sigma_t^d b^d(t, T) \right)^2 \right] dt - \sigma_t^d b^d(t, T) dW_t^{d(\text{T})}, \\
\frac{dP^f(t, T)}{P^f(t, T)} &= \left[r_t^f + \sigma_t^f b^f(t, T) \left(\rho_{Sf} \sigma^S + \rho_{df} \sigma_t^d b^d(t, T) \right) \right] dt \\
&\quad - \sigma_t^f b^f(t, T) dW_t^{f(\text{T})}.
\end{aligned} \tag{5.3}$$

Similarly, the exchange rate process written in the domestic T -forward measure is given by (c.f. (2.14))

$$dS_t = \left[r_t^d - r_t^f - \rho_{Sd} b^d(t, T) \sigma_t^d \sigma^S \right] S_t dt + \sigma^S S_t dW_t^{S(\text{T})}. \tag{5.4}$$

The forward value of the exchange rate is

$$F(t, T) \equiv \mathbf{E}^{\mathbb{Q}(\text{T})} [S_T \mid \mathcal{F}_t] = S_t \frac{P^f(t, T)}{P^d(t, T)}, \tag{5.5}$$

which is a martingale under the T -forward measure $\mathbb{Q}^{(T)}$. Its SDE can be computed from (5.3), (5.4), and application of Itô's lemma,

$$\frac{dF(t, T)}{F(t, T)} = \sigma^S dW_t^{S(T)} + \sigma_t^d b^d(t, T) dW_t^{d(T)} - \sigma_t^f b^f(t, T) dW_t^{f(T)}. \quad (5.6)$$

Since the diffusion process above is a linear combination of correlated Brownian motions, we can extract the total implied variance easily,

$$\begin{aligned} \Sigma^2 T = & (\sigma^S)^2 T + 2\sigma^S \int_0^T \left[\rho_{Sd} \sigma_t^d b^d(t, T) - \rho_{Sf} \sigma_t^f b^f(t, T) \right] dt \\ & + \int_0^T \left[(\sigma_t^d b^d(t, T))^2 - 2\rho_{df} \sigma_t^d b^d(t, T) \sigma_t^f b^f(t, T) + (\sigma_t^f b^f(t, T))^2 \right] dt. \end{aligned} \quad (5.7)$$

With this quantity one can write down the Black formula for the time zero value of a vanilla call option as

$$C(K, T) = P^d(0, T) \left[F(0, T) N(\tilde{d}_1) - KN(\tilde{d}_2) \right], \quad (5.8)$$

with $\tilde{d}_1 = \frac{\log \frac{F(0, T)}{K} + \frac{1}{2} \Sigma^2 T}{\Sigma \sqrt{T}}$ and $\tilde{d}_2 = \tilde{d}_1 - \Sigma \sqrt{T}$.

The integrals in (5.7) can be evaluated numerically. Therefore, for a given market implied volatility Σ at a given maturity T and strike K , one can solve this quadratic equation to find the BS2SR volatility σ^S that will reproduce the market quotes. Conversely, the right hand side of (5.7) dictates the lower bound of total implied variance for which there is a solution for the BS2SR model. The lower bound can be evaluated, by taking the derivative with respect to σ^S and setting it to zero,

$$\begin{aligned} \Sigma_{\min}^2 T = & \int_0^T \left[(\sigma_t^d b^d(t, T))^2 - 2\rho_{df} \sigma_t^d b^d(t, T) \sigma_t^f b^f(t, T) + (\sigma_t^f b^f(t, T))^2 \right] dt \\ & - \frac{1}{T} \left(\int_0^T \left[\rho_{Sd} \sigma_t^d b^d(t, T) - \rho_{Sf} \sigma_t^f b^f(t, T) \right] dt \right)^2. \end{aligned} \quad (5.9)$$

If the market total implied variance at a given maturity T and strike K is lower than this, the BS2SR model will not have a solution. As a consequence, the local volatility extension of this model (LV2SR) will not be calibratable, that is the evaluation of (2.18) during the application of the calibration algorithm will lead to imaginary values for local volatility given the already fixed parameters of the interest rate models and the correlations. This signifies that no real and positive local volatility exists that would reproduce the market quotes for vanilla options within such a model.

As a study, we take the market data as of 2020-04-30, but vary the interest rate model parameters and correlations, and compare the minimum total implied variance admitted by the BS2SR model for a number of values of interest rate volatilities and correlations. In particular for a mean reversion $a_t^d = a_t^f = 0.01$, and volatilities $\sigma_t^d = \sigma_t^f = 0.02, 0.05$ we look at the minimum total implied variances admitted by the BS2SR model for various values of ρ_{df} . Figure 5.3 shows that for interest rate volatilities set to 0.02, the market total implied variance is lower than the minimum total implied variance admitted by the BS2SR model at various strikes when the correlation ρ_{df} is below -0.4. In case the interest rate volatilities are set to 0.05, the market total implied variance is attainable only when the correlation ρ_{df} is quite high, around 0.8.

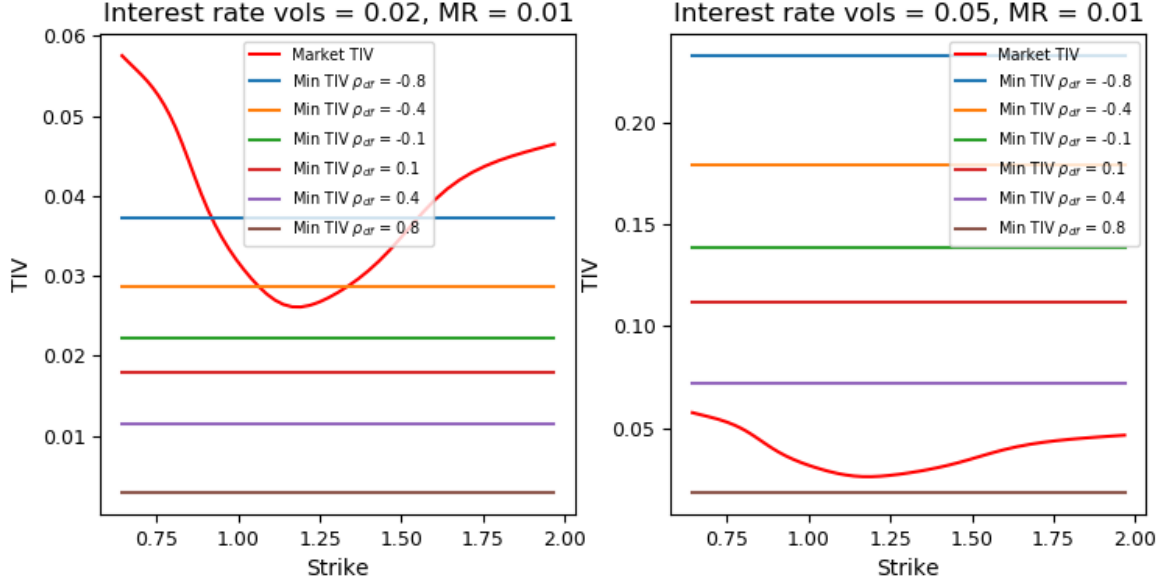


Figure 5.3: Minimum total implied variances (TIV) allowed by the BS2SR model for various values of interest rate volatilities and correlations compared to market TIV. $\rho_{Sd} = 0.166$, $\rho_{Sf} = 0.551$

A Supplementary computations

The following finding is utilized in measure transformations throughout the paper.

Lemma A.1. *Let*

$$dX_t = a(X_t, t)dt + b(X_t, t)dW_t^{X(A)}, \quad (\text{A.1})$$

with

$$P \left(\int_0^t (|a(X_s, s)| + |b^2(X_s, s)|) ds < \infty \right) = 1, \quad \forall t \geq 0,$$

be an SDE describing the evolution of process (X_t) under measure \mathbb{Q}^A whose Brownian motion $(W_t^{X(A)})$ is correlated to another Brownian motion $(W_t^{Y(A)})$ with a coefficient of correlation ρ_{XY} , that is $d\langle W^{X(A)}, W^{Y(A)} \rangle_t = \rho_{XY}dt$. Let $(W_t^{Y(B)})$ be a Brownian motion under an equivalent measure \mathbb{Q}^B characterized by the transformation

$$\frac{d\mathbb{Q}^B}{d\mathbb{Q}^A} = \exp \left[-\frac{1}{2} \int_0^t c^2(\cdot, s)ds - \int_0^t c(\cdot, s)dW_s^{Y(A)} \right], \quad (\text{A.2})$$

such that

$$dW_t^{Y(B)} = dW_t^{Y(A)} + c(\cdot, t)dt, \quad (\text{A.3})$$

with $P \left(\int_0^t |c(\cdot, s)| ds < \infty \right) = 1, \quad \forall t \geq 0$, and $c(\cdot, t)$ is a function of underlying assets of the SDE system, and time. Then the evolution of (X_t) under measure \mathbb{Q}^B is described by

$$dX_t = [a(X_t, t) - \rho_{XY}b(X_t, t)c(\cdot, t)]dt + b(X_t, t)dW_t^{X(B)}, \quad (\text{A.4})$$

where $(W_t^{X(B)})$ is a Brownian motion under \mathbb{Q}^B .

Proof. We can decompose the Brownian motion $(W_t^{X(A)})$ into $(W_t^{Y(A)})$ and an independent Brownian motion (Z_t) , that is $d\langle W^{Y(A)}, Z \rangle_t = 0$, as

$$dW_t^{X(A)} = \rho_{XY} dW_t^{Y(A)} + \sqrt{1 - \rho_{XY}^2} dZ_t. \quad (\text{A.5})$$

We note that, as a result of the multi-dimensional Girsanov theorem, (Z_t) is a Brownian motion under \mathbb{Q}^B .

Now we can use (A.3) and (A.5) to write the process (A.1) as

$$\begin{aligned} dX_t &= a(X_t, t)dt + b(X_t, t) \left[\rho_{XY} dW_t^{Y(A)} + \sqrt{1 - \rho_{XY}^2} dZ_t \right] \\ &= a(X_t, t)dt + b(X_t, t) \left[\rho_{XY} \left(dW_t^{Y(B)} - c(\cdot, t)dt \right) + \sqrt{1 - \rho_{XY}^2} dZ_t \right] \\ &= [a(X_t, t) - \rho_{XY} b(X_t, t)c(\cdot, t)] dt + b(X_t, t) dW_t^{X(B)}, \end{aligned} \quad (\text{A.6})$$

with

$$\begin{aligned} dW_t^{X(B)} &= \rho_{XY} dW_t^{Y(B)} + \sqrt{1 - \rho_{XY}^2} dZ_t \\ &= dW_t^{X(A)} + \rho_{XY} c(\cdot, t)dt. \end{aligned} \quad (\text{A.7})$$

□

We use the following result during the change to T -forward measure in Section 2.1.2. The limiting case with constant coefficients was investigated in [30]. Here we study the general case with time dependent coefficients.

Lemma A.2. *For the G1++ model (2.2) describing the evolution of the short rate (r_t) ,*

$$\begin{aligned} r_t &= x_t + \phi_t, \\ dx_t &= -a_t x_t dt + \sigma_t dW_t, \end{aligned} \quad (\text{A.8})$$

where ϕ_t is the deterministic shift function that is calibrated to market yield curve; a_t is the mean reversion coefficient, and σ_t is the volatility coefficient, the following identity holds,

$$\exp \left[- \int_t^T r_s ds \right] = P(t, T) \exp \left[- \int_t^T \sigma_v b(v, T) dW_v - \frac{1}{2} \int_t^T \sigma_v^2 b^2(v, T) dv \right]. \quad (\text{A.9})$$

Here, $P(t, T) \equiv \mathbf{E} \left[e^{-\int_t^T r_s ds} | \mathcal{F}_t \right]$ is the time t value of a zero coupon bond maturing at time T , and $b(t, T) \equiv \int_t^T e^{-\int_t^v a_z dz} dv$.

Proof. The integral on the left hand side of (A.9) can be split into $-\int_t^T r_s ds = -\int_t^T x_s ds - \int_t^T \phi_s ds$. We start with integrating the first of these integrals by parts,

$$\begin{aligned} \int_t^T x_s ds &= s x_s \Big|_t^T - \int_t^T s dx_s \\ &= (T - t)x_t + \int_t^T (T - v)(-a_v x_v dv + \sigma_v dW_v). \end{aligned} \quad (\text{A.10})$$

We compute x_s by evaluating the following integral

$$\int_t^s du \left(x_u e^{\int_t^u a_z dz} \right) = \int_t^s a_u e^{\int_t^u a_z dz} x_u du + \int_t^s e^{\int_t^u a_z dz} (-a_u x_u du + \sigma_u dW_u),$$

which leads to

$$x_s = x_t e^{-\int_t^s a_z dz} + \int_t^s e^{-\int_t^u a_z dz} \sigma_u dW_u. \quad (\text{A.11})$$

We plug this into (A.10) to get

$$\begin{aligned} \int_t^T x_s ds &= (T-t)x_t - x_t \int_t^T (T-v)a_v e^{-\int_t^v a_z dz} dv \\ &\quad + \int_t^T (T-v) \left[-a_v \left(\int_t^v e^{-\int_t^u a_z dz} \sigma_u dW_u \right) dv + \sigma_v dW_v \right]. \end{aligned}$$

The first two integrals appearing in the right hand side above can be evaluated by integration by parts. The first one yields

$$\begin{aligned} - \int_t^T (T-v)a_v e^{-\int_t^v a_z dz} dv &= (T-v)e^{-\int_t^v a_z dz} \Big|_{v=t}^T + \int_t^T e^{-\int_t^v a_z dz} dv \\ &= -(T-t) + b(t, T). \end{aligned}$$

The second one evaluates

$$\begin{aligned} &- \int_t^T (T-v)a_v \int_t^v e^{-\int_t^u a_z dz} \sigma_u dW_u dv \\ &= - \int_t^T \left(\int_t^v e^{\int_t^u a_z dz} \sigma_u dW_u \right) dv \left(\int_t^v a_y (T-y) e^{-\int_t^y a_z dz} dy \right) \\ &= - \left[\int_t^v e^{\int_t^u a_z dz} \sigma_u dW_u \int_t^v a_y (T-y) e^{-\int_t^y a_z dz} dy \right]_{v=t}^T \\ &\quad + \int_t^T e^{\int_t^v a_z dz} \sigma_v dW_v \int_t^v a_y (T-y) e^{-\int_t^y a_z dz} dy \\ &= - \int_t^T e^{\int_t^v a_z dz} \sigma_v dW_v \int_v^T a_y (T-y) e^{-\int_t^y a_z dz} dy \\ &= \int_t^T [-(T-v) + b(v, T)] \sigma_v dW_v. \end{aligned}$$

This leads to

$$\int_t^T x_s ds = x_t b(t, T) + \int_t^T \sigma_v b(v, T) dW_v. \quad (\text{A.12})$$

Hence

$$\begin{aligned} \mathbf{E} \left[\int_t^T x_u du \right] &= x_t b(t, T) \\ \mathbf{Var} \left[\int_t^T x_u du \right] &= \int_t^T \sigma_v^2 b^2(t, T) dv. \end{aligned}$$

Since $\mathbf{E} [e^{-X}] = e^{-\mu + \frac{1}{2}\sigma^2}$ where $X \sim N(\mu, \sigma^2)$, we have

$$\begin{aligned} P(t, T) &= \mathbf{E} \left[e^{-\int_t^T (\phi_s + x_s) ds} \middle| \mathcal{F}_t \right] = e^{-\int_t^T \phi_s ds - x_t b(t, T) + \frac{1}{2} \int_t^T \sigma_v^2 b^2(v, T) dv} \\ &= e^{\int_t^T x_s ds} e^{-\int_t^T r_s ds} e^{-x_t b(t, T) + \frac{1}{2} \int_t^T \sigma_v^2 b^2(v, T) dv}. \end{aligned}$$

Plugging in (A.12) into this expression gives the desired result. \square

Lemma A.3. *Let*

$$dS_t = (r_t^d - r_t^f) S_t dt + \sigma_S(t, S_t, U_t) S_t dW_t^{S(DRN)} \quad (\text{A.13})$$

be an SDE describing the evolution of asset process (S_t) under the domestic risk neutral measure \mathbb{Q}^{DRN} associated with the money market numéraire $B_t^d = \exp[\int_0^t r_s^d ds]$; (r_t^d) , (r_t^f) and (U_t) be stochastic processes. Let $C(K, T)$ be the price of a vanilla call option written on (S_t) , with strike K and maturity T , so that $C(K, T) = \mathbf{E}^{\mathbb{Q}^{DRN}} \left[\frac{1}{B_T^d} (S_T - K)^+ \right]$. Then the following identity holds

$$\mathbf{E}^{\mathbb{Q}^T} \left[\sigma_S^2(T, S_T, U_T) \middle| S_T = K \right] = \frac{\frac{\partial C}{\partial T} - P^d(0, T) \mathbf{E}^{\mathbb{Q}^T} \left[(r_T^d K - r_T^f S_T) \mathbf{1}_{S_T > K} \right]}{\frac{1}{2} K^2 \frac{\partial^2 C}{\partial K^2}},$$

where the expectations are taken under the T -forward measure \mathbb{Q}^T associated with the zero coupon bond price numéraire $P^d(0, T) = \mathbf{E}^{\mathbb{Q}^{DRN}} \left[\frac{1}{B_T^d} \right]$.

Proof. Here we apply the methodology from Section 10.2.1 of [31] to our setup. The Tanaka-Meyer formula for the positive part function for a continuous semimartingale states in differential form

$$d(S_t - K)^+ = \mathbf{1}_{S_t > K} dS_t + \frac{1}{2} \delta(S_t - K) d\langle S \rangle_t,$$

with $\langle \cdot \rangle_s$ being the quadratic variation, and δ being the Dirac delta distribution, possibly characterized as a limit. We will later take expectations, so we are only interested in the drift term. Applying (A.13) into this, we obtain that the drift term of $d(S_t - K)^+$ as

$$\mathbf{1}_{S_t > K} (r_t^d - r_t^f) S_t + \frac{1}{2} \delta(S_t - K) \sigma_S^2(t, S_t, U_t) S_t^2.$$

We use the product rule to compute the drift term of the discounted payoff $d \left[\frac{1}{B_t^d} (S_t - K)^+ \right]$ as

$$\frac{1}{B_t^d} \left(-r_t^d (S_t - K)^+ + \mathbf{1}_{S_t > K} (r_t^d - r_t^f) S_t + \frac{1}{2} \delta(S_t - K) \sigma_S^2(t, S_t, U_t) S_t^2 \right),$$

which we simplify, using $(S_t - K)^+ = \mathbf{1}_{S_t > K} (S_t - K)$, to

$$\frac{1}{B_t^d} \left(\mathbf{1}_{S_t > K} (r_t^d K - r_t^f S_t) + \frac{1}{2} \delta(S_t - K) \sigma_S^2(t, S_t, U_t) S_t^2 \right).$$

We take the expectation under the domestic risk neutral measure $\mathbf{E}^{\mathbb{Q}^{\text{DRN}}}$, noting the fact that the expression inside the differential is the value of the vanilla call option with strike K and maturity T , and assuming the diffusion term is a true martingale, to arrive at

$$\begin{aligned}\frac{\partial C}{\partial T} &= \mathbf{E}^{\mathbb{Q}^{\text{DRN}}} \left[\frac{1}{B_T^d} \left(\mathbf{1}_{S_T > K} (r_T^d K - r_T^f S_T) + \frac{1}{2} \delta (S_T - K) \sigma_S^2(T, S_T, U_T) S_T^2 \right) \right] \\ &= P^d(0, T) \mathbf{E}^{\mathbb{Q}^T} \left[\mathbf{1}_{S_T > K} (r_T^d K - r_T^f S_T) + \frac{1}{2} \delta (S_T - K) \sigma_S^2(T, S_T, U_T) S_T^2 \right]\end{aligned}$$

We first consider

$$\begin{aligned}\mathbf{E}^{\mathbb{Q}^T} [\delta (S_T - K) \sigma_S^2(T, S_T, U_T) S_T^2] &= \mathbf{E}^{\mathbb{Q}^T} \left[\mathbf{E}^{\mathbb{Q}^T} [\sigma_S^2(T, S_T, U_T) | S_T] \delta (S_T - K) S_T^2 \right] \\ &= q^T(K, T) K^2 \mathbf{E}^{\mathbb{Q}^T} [\sigma_S^2(T, S_T, U_T) | S_T = K]\end{aligned}$$

where we used the properties of conditional expectations, and denoted the marginal distribution of (S_T) under the T -forward measure with $q^T(S_T, T)$. Now we use [32] relationship $\frac{\partial^2 C}{\partial K^2} = P^d(0, T) q^T(K, T)$ to rewrite

$$\begin{aligned}\frac{\partial C}{\partial T} &= P^d(0, T) \mathbf{E}^{\mathbb{Q}^T} \left[\mathbf{1}_{S_T > K} (r_T^d K - r_T^f S_T) \right] \\ &\quad + \frac{1}{2} K^2 \frac{\partial^2 C}{\partial K^2} \mathbf{E}^{\mathbb{Q}^T} [\sigma_S^2(T, S_T, U_T) | S_T = K]\end{aligned}$$

□

For the LV2SR model, $\sigma_S(t, S_t, U_t) = \sigma_{LV}(S_t, t)$, thus the second expectation simplifies to $\sigma_{LV}^2(K, T)$ and we obtain

$$\frac{\partial C}{\partial T} = P^d(0, T) \mathbf{E}^{\mathbb{Q}^T} \left[\mathbf{1}_{S_T > K} (r_T^d K - r_T^f S_T) \right] + \frac{1}{2} K^2 \frac{\partial^2 C}{\partial K^2} \sigma_{LV}^2(K, T). \quad (\text{A.14})$$

For the SLV2SR model, $\sigma_S^2(t, S_t, U_t) = L^2(S_t, t) U_t$, thus the second expectation factors to $L^2(K, T) \mathbf{E}^{\mathbb{Q}^T} [U_T | S_T = K]$ and we obtain

$$\begin{aligned}\frac{\partial C}{\partial T} &= P^d(0, T) \mathbf{E}^{\mathbb{Q}^T} \left[\mathbf{1}_{S_T > K} (r_T^d K - r_T^f S_T) \right] \\ &\quad + \frac{1}{2} K^2 \frac{\partial^2 C}{\partial K^2} L^2(K, T) \mathbf{E}^{\mathbb{Q}^T} [U_T | S_T = K].\end{aligned} \quad (\text{A.15})$$

We can rewrite (A.14) as

$$\sigma_{LV}^2(K, T) = \frac{\frac{\partial C}{\partial T} - P^d(0, T) \mathbf{E}^{\mathbb{Q}^T} \left[(r_T^d K - r_T^f S_T) \mathbf{1}_{S_T > K} \right]}{\frac{1}{2} K^2 \frac{\partial^2 C}{\partial K^2}}. \quad (\text{A.16})$$

In the total implied variance parametrization of the Black-Scholes model, using identities

(2.21) together with

$$\begin{aligned}
\frac{\partial^2 C_{BS}}{\partial w^2} &= \frac{1}{2} \frac{\partial C_{BS}}{\partial w} \left[-\frac{1}{4} - \frac{1}{w} + \frac{y^2}{w^2} \right], \\
\frac{\partial^2 C_{BS}}{\partial w \partial y} &= \frac{\partial C_{BS}}{\partial w} \left[-\frac{y}{w} + \frac{1}{2} \right], \\
\frac{\partial^2 C_{BS}}{\partial y^2} &= \frac{\partial C_{BS}}{\partial y} + 2 \frac{\partial C_{BS}}{\partial w},
\end{aligned} \tag{A.17}$$

one derives

$$\begin{aligned}
K^2 \frac{\partial^2 C_{BS}}{\partial K^2} &= \frac{\partial^2 C_{BS}}{\partial y^2} + \left(2 \frac{\partial^2 C_{BS}}{\partial w \partial y} + \frac{\partial^2 C_{BS}}{\partial w^2} \frac{\partial w}{\partial y} - \frac{\partial C_{BS}}{\partial w} \right) \frac{\partial w}{\partial y} \\
&\quad + \frac{\partial C_{BS}}{\partial w} \frac{\partial^2 w}{\partial y^2} - \frac{\partial C_{BS}}{\partial y} \\
&= 2 \frac{\partial C_{BS}}{\partial w} \left[1 - \frac{y}{w} \frac{\partial w}{\partial y} + \frac{1}{2} \frac{\partial^2 w}{\partial y^2} + \frac{1}{4} \left(\frac{\partial w}{\partial y} \right)^2 \left(-\frac{1}{4} - \frac{1}{w} + \frac{y^2}{w^2} \right) \right].
\end{aligned} \tag{A.18}$$

Therefore in this parametrization (A.16) can be written as

$$\sigma_{LV}^2(K, T) = \frac{\frac{\partial C_{BS}}{\partial T} - P^d(0, T) \mathbf{E}^{\mathbb{Q}^T} \left[(r_T^d K - r_T^f S_T) \mathbf{1}_{S_T > K} \right]}{\frac{\partial C_{BS}}{\partial w} \left[1 - \frac{y}{w} \frac{\partial w}{\partial y} + \frac{1}{2} \frac{\partial^2 w}{\partial y^2} + \frac{1}{4} \left(\frac{\partial w}{\partial y} \right)^2 \left(-\frac{1}{4} - \frac{1}{w} + \frac{y^2}{w^2} \right) \right]}, \tag{A.19}$$

where $\frac{\partial C_{BS}}{\partial T}$ and $\frac{\partial C_{BS}}{\partial w}$ are as given in (2.21).

Notice that (A.16) can be computed for any SDE system that includes the given SDE subsystems for (S) , (r^d) and (r^f) . In particular, one can compute such a ‘‘local volatility’’ even for stochastic local volatility models. (A.15) can be reformulated as [22]

$$L^2(K, T) \mathbf{E}^{\mathbb{Q}^T} [U_T | S_T = K] = \frac{\frac{\partial C}{\partial T} - P^d(0, T) \mathbf{E}^{\mathbb{Q}^T} \left[(r_T^d K - r_T^f S_T) \mathbf{1}_{S_T > K} \right]}{\frac{1}{2} K^2 \frac{\partial^2 C}{\partial K^2}}, \tag{A.20}$$

and by comparing this to (A.16) we arrive at the relationship between the SLV2SR model leverage function and the LV2SR submodel local volatility function,

$$L^2(K, T) = \frac{\sigma_{LV}^2(K, T)}{\mathbf{E}^{\mathbb{Q}^T} [U_T | S_T = K]}. \tag{A.21}$$

Acknowledgments The authors are grateful to the reviewers and the editor for their valuable comments that have helped us improve the paper substantially. The authors are indebted to Dooheon Lee and Kisun Yoon for numerous enlightening discussions and guidance about the theoretical foundations of this paper. The authors would also like to thank Agus Sudjianto for supporting this research, and Vijayan Nair for suggestions, feedback, and discussion regarding this work. Any opinions, findings and conclusions or recommendations expressed in this material are those of the authors and do not necessarily reflect the views of Wells Fargo Bank, N.A., its parent company, affiliates and subsidiaries.

References

- [1] Bruno Dupire. Pricing with a Smile. *Risk Magazine*, pages 18–20, January 1994.
- [2] Emanuel Derman and Iraj Kani. Riding on a Smile. *Risk Magazine*, pages 32–39, February 1994.
- [3] Marc Atlan. Localizing Volatilities, 2006. arXiv:math/0604316.
- [4] Bing Hu. Local Volatility Model with Stochastic Interest Rate. Master’s thesis, York University, August 2015.
- [5] Julien Hok and Shih-Hau Tan. Calibration of Local Volatility Model with Stochastic Interest Rates by Efficient Numerical PDE Method. *Decisions in Economics and Finance*, 42:609–637, 2019.
- [6] Griselda Deelstra and Grégory Rayée. Local Volatility Pricing Models for Long-dated FX Derivatives. *Applied Mathematical Finance*, 20(1204.0633):380 – 402, 2013.
- [7] Steven L. Heston. A Closed-Form Solution for Options with Stochastic Volatility with Applications to Bond and Currency Options. *The Review of Financial Studies*, 6(2):327–343, 04 1993.
- [8] John C. Cox, Jonathan E. Ingersoll, and Stephen A. Ross. A Theory of the Term Structure of Interest Rates. *Econometrica*, 53(2):385–407, 1985.
- [9] Elias M. Stein and Jeremy C. Stein. Stock Price Distributions with Stochastic Volatility: An Analytic Approach. *Review of Financial Studies*, 4:727–752, 1991.
- [10] Rainer Schöbel and Jianwei Zhu. Stochastic Volatility With an Ornstein-Uhlenbeck Process: An Extension. *Review of Finance*, 3(1):23–46, 04 1999.
- [11] G. E. Uhlenbeck and L. S. Ornstein. On the Theory of the Brownian Motion. *Phys. Rev.*, 36:823–841, Sep 1930.
- [12] Bruno Dupire. A unified theory of volatility. In *Discussion paper Paribas Capital Markets, reprinted in "Derivatives Pricing: The Classic Collection"*, edited by Peter Carr, 2004, pages 185–196. Risk Books, London, 1996.
- [13] Carol Alexander and Leonardo M. Nogueira. Stochastic local volatility. In *Proceedings of the Second IASTED International Conference on Financial Engineering and Applications*, pages 136–141, November 8-10, Cambridge, MA, USA, 2004.
- [14] Alexander Lipton. The vol smile problem. *Risk Magazine*, 15(2):61–66, February 2002.
- [15] Michal Jex, R. C. W. Henderson, and Desheng Wang. Pricing Exotics Under the Smile. *Risk*, 12:72–75, 01 1999.
- [16] J. Guyon and P. Henry-Labordère. *Nonlinear Option Pricing*, volume 1 of *Chapman and Hall/CRC Financial Mathematics Series*. CRC Press, 2013.

- [17] Y. Ren, D. Madan, and M. Q. Qian. Calibrating and Pricing with Embedded Local Volatility Models. *Risk*, pages 138–143, September 2007.
- [18] Yuri F. Saporito, Xu Yang, and Jorge P. Zubelli. The Calibration of Stochastic-Local Volatility Models - An Inverse Problem Perspective. *Computers & Mathematics with Applications*, 77(12):3054–3067, 2019.
- [19] P. Henry-Labordère. Calibration of local stochastic volatility models to market smiles: A monte-carlo approach. *Derivatives*, 2009.
- [20] S.E. Shreve. *Stochastic Calculus for Finance II: Continuous-Time Models*, volume 2 of *Springer Finance Textbooks*. Springer, 2004.
- [21] Jim Gatheral. *The Volatility Surface*, chapter 1, pages 1–14. John Wiley & Sons, Ltd, 2012.
- [22] Orcan Ogetbil. Extensions of Dupire Formula: Stochastic Interest Rates and Stochastic Local Volatility, 2020. arXiv:2005.05530.
- [23] Sébastien Gurrieri, Masaki Nakabayashi, and Tony Wong. Calibration methods of Hull-White model. *Available at SSRN 1514192*, 2009.
- [24] Sergei Mikhailov and Ulrich Nögel. Heston’s Stochastic Volatility Model Implementation, Calibration and Some Extensions. *Willmott Magazine*, 1:74–79, 2005.
- [25] Daniel Guterding and Wolfram Boenkost. The Heston stochastic volatility model with piecewise constant parameters - efficient calibration and pricing of window barrier options. *Journal of Computational and Applied Mathematics*, 343:353 – 362, 2018.
- [26] Sensen Lin. Finite difference schemes for heston model. Master’s thesis, The University of Oxford, 2008.
- [27] William Feller. Two Singular Diffusion Problems. *Annals of Mathematics*, 54(1):173–182, 1951.
- [28] J. A. Nelder and R. Mead. A Simplex Method for Function Minimization. *The Computer Journal*, 7(4):308–313, 01 1965.
- [29] Paul Wilmott. *Paul Wilmott on Quantitative Finance*. John Wiley & Sons, 2013.
- [30] D. Brigo and F. Mercurio. *Interest Rate Models Theory and Practice*, volume 1 of *Springer Finance*. Springer Berlin Heidelberg, 2013.
- [31] Cornelis W Oosterlee and Lech A Grzelak. *Mathematical Modeling and Computation in Finance: With Exercises and Python and Matlab Computer Codes*. World Scientific, 2019.
- [32] Douglas T Breeden and Robert H Litzenberger. Prices of state-contingent claims implicit in option prices. *The Journal of Business*, 51(4):621–51, 1978.